



Michigan Technological University
Create the Future Digital Commons @ Michigan Tech

Dissertations, Master's Theses and Master's
Reports - Open

Dissertations, Master's Theses and Master's
Reports

2011

Nitrogen oxides in the firn air at Summit, Greenland

Claudia Toro
Michigan Technological University

Follow this and additional works at: <https://digitalcommons.mtu.edu/etds>



Part of the [Civil and Environmental Engineering Commons](#)

Copyright 2011 Claudia Toro

Recommended Citation

Toro, Claudia, "Nitrogen oxides in the firn air at Summit, Greenland", Master's Thesis, Michigan Technological University, 2011.
<https://doi.org/10.37099/mtu.dc.etds/276>

Follow this and additional works at: <https://digitalcommons.mtu.edu/etds>



Part of the [Civil and Environmental Engineering Commons](#)

NITROGEN OXIDES IN THE FIRN AIR AT SUMMIT, GREENLAND

By

Claudia Toro

A THESIS

Submitted in partial fulfillment of the requirements for the degree of

MASTER OF SCIENCE

(Environmental Engineering Science)

MICHIGAN TECHNOLOGICAL UNIVERSITY

2011

© 2011 Claudia Toro

This thesis, “Nitrogen Oxides In The Firn Air At Summit, Greenland ,” is hereby approved in partial fulfillment for the requirements for the degree of MASTER OF SCIENCE IN ENVIRONMENTAL ENGINEERING SCIENCE.

Department of Civil and Environmental Engineering

Advisor: _____
Dr. Paul V. Doskey

Committee Member: _____
Dr. Louisa J. Kramer

Committee Member: _____
Dr. Sarah A. Green

Department Chair: _____
Dr. David W. Hand

Date: _____

CONTENTS

List of Figures	viii
Acknowledgments	ix
Abstract	xi
1 Introduction	1
2 Background	5
2.1 Transport mechanisms and physical properties of snow relevant to snow photochemistry	5
2.2 Photochemistry at high latitudes	6
2.3 The quasi-liquid layer	7
2.4 Reactive species in snow photochemistry	9
2.4.1 Nitrate	9
2.4.2 Nitrogen oxides	11
2.4.3 Nitrous acid	12
2.5 Halogens	13
2.6 Ozone	13
2.7 HO_X	14
2.8 Implications of snowpack photochemistry	15
3 Research Design and Methods	17
3.1 Site Description	17
3.2 Experimental Setup	18
3.2.1 Met-tower	19
3.2.2 Snow-tower	19
3.3 Sampling Technique	21
3.4 Measurement Technique	22
3.4.1 Measurement Cycle	22
3.4.2 NO measurement	23

3.4.3	NO ₂ measurement	24
3.4.4	Uncertainties of NO/NO ₂ measurements	24
3.4.5	Calibration	25
3.5	Data Analysis	26
3.5.1	NO _x measurements correction	26
3.5.2	Data Screening	30
3.6	Ancillary measurements	32
3.6.1	Ozone	32
3.6.2	Wind speed and direction	32
3.6.3	Radiation	32
3.6.4	Snowpack Temperature	33
4	Results and Discussion	35
4.1	Seasonal characteristics	35
4.1.1	Wind influence on NO _x distribution within the snow	40
4.1.2	Influence of snowpack temperature	44
4.1.3	NO and NO ₂ profiles.	45
4.2	Diurnal Cycles	50
5	Conclusions and Future Work	57
5.1	Conclusions	58
5.2	Future work	61
	References	73
	Appendices	75
A	Schematics	77
B	Derivation of relevant equations used for this work.	81
B.1	Derivation of the Equation for Calculating the NO ₂ Sensitivity	81
B.2	Derivation of the Equation for Correcting NO Sensitivity.	85

LIST OF FIGURES

1.1	Physical and chemical processes involved in snowpack photochemistry at polar regions.	2
3.1	Geographical location of Summit Station	18
3.2	Experimental Setup	20
3.3	Correlation plot and time series of one of the periods selected for correcting sensitivity.	28
3.4	Time series of NO sensitivity	29
3.5	Magnitude of NO correction at different levels within the snow	31
4.1	Daily averages of NO _x mixing ratios within and above the snowpack between June 2008 and July 2010	36
4.2	Contour plot of NO _x mixing ratios within the snowpack for each year.	39
4.3	Daily averages of NO _x in the snowpack and daily averages of wind speed 2009.	41
4.4	Daily averages of NO _x in the snowpack and daily averages of wind speed 2010.	42
4.5	Diurnal averages of snowpack temperature.	44
4.6	Daily averages of NO ₂ and NO for year 2009 and 2010. Black dashed line represents the surface of the snowpack.	46
4.7	Daily average of O ₃ mixing ratios within and above the snowpack between June 2008 and July 2010.	47
4.8	Daily averages of NO ₂ (top) and NO (bottom) enhancements (respect to ambient concentrations) within the snow for 2009 and 2010 seasons at levels of photochemical activity.	49
4.9	Box plots of NO _x enhancements within the snow for three different depths, showing the average diurnal cycle for each month during spring-summer 2009.	51
4.10	Box plots of NO ₂ and NO enhancements within the snow for 2 levels, showing the average diurnal cycle for each month during spring-summer 2009.	53

A.1	Detailed Schematic of the Experimental Setup	79
A.2	Flow diagrams	80

ACKNOWLEDGMENTS

I would like to thank to my advisor and committee members, Dr. Paul Doskey, Dr. Sarah Green and specially to Dr. Louisa Kramer for her incredible support, infinite understanding and fully involvement in this project. Without her participation and commitment after Dr. Honrath passed away, this project would not have reached its current state of development, and certainly I would not have been able to keep going. I also would like to thank to Brie Van Dam for her time preparing data and kindly allowing me to use her figures, training me in Summit and for the valuable discussions about snow and life. Her attitude to face problems inspired me to improve my own. I also would like to thanks to Dr. Raymond Shaw for his time and valuable discussions about my career options. Special thanks to the NSF project ARC0713943 for funding my studies.

Finally, I want to thank to my family and friends, and specially to Buddy for helping me to go through one of the most difficult situations of my life. Thanks for being there.

ABSTRACT

Measurements of NO_x within the snowpack at Summit, Greenland were carried out from June 2008 to July 2010, using a novel system to sample firn air with minimal disruption of the snowpack. These long-term measurements were motivated by the need of improving the representation of air-snow interactions in global models. Results indicated that the NO_x budget within the snowpack was on the order of 550 pptv as maximum, and was constituted primarily for NO_2 . NO_x production was observed within the first 50 cm of the snowpack during the sunlight season between February and August. Presence of NO_x at larger depths was attributed to high speed wind and vertical transport processes. Production of NO correlated with the seasonal incoming radiation profile, while NO_2 maximum was observed in April. These measurements constitute the larger data set of NO_x within the firn and will improve the representation of processes driving snow photochemistry at Summit.

1. INTRODUCTION

An increasing number of studies have demonstrated that snow is not as chemically pristine as might be thought. In fact, snow plays a significant role in the chemistry of the atmosphere above it. In polar regions as well as in mid latitude areas, snowpacks can act both as a sink and as a source for many trace gases of relevance to atmospheric chemistry.

Chemical species can be deposited into the snowpack by any of the following deposition mechanisms: wet, fog or dry deposition. In addition, (photo)chemical reactions can have an impact on deposited chemical species and alter their concentrations in the *firn*. The *firn* corresponds to the first tens of meters of the snowpack and is simply snow that has not melted through the years and is being compacted into ice. The exchange of gases between the snowpack and the atmosphere depends greatly on the chemical composition and physical characteristics of the firn *.

Physical properties of the snow such as diffusivity, porosity, permeability and snow grain geometry affect transport processes through the snowpack. Two physical mechanisms that causes chemical changes in the surface snow are diffusion and ventilation, and in particular, thermal and chemical gradients are the driving force for any exchange of species between the snowpack and the overlying atmosphere.

Nitrogen oxides ($\text{NO}_x = \text{NO} + \text{NO}_2$) control the oxidative capacity of the atmosphere through ozone (O_3) production. In urban areas, NO_x are considered primary pollutants since their sources are mainly combustion of fossil fuels. From the point of view of air quality, they constitute a threat to public health for their role in the formation of photochemical smog.

*Through the rest of this work, the term snowpack will refer specifically to the firn section of it.

In remote areas, particularly in polar regions, nitrogen oxides were expected to be very low. The discovery of elevated NO_x mixing ratios within the snowpack at Summit, Greenland (1) demonstrated that snowpacks are actually a photochemically active reactor. Evidence pointed towards the photolysis of nitrate (NO_3^-) previously deposited in the snow as the most likely NO_x source, bringing into question how these snowpack processes would affect the interpretation of nitrate ice-cores (2–4).

Since then, a number of campaigns have focused on snow photochemistry in a variety of locations: Arctic (5–11), Antarctic (12–17) and midlatitudes (18–20). All of them have concluded that snowpacks are an active environment where physical exchange processes, heterogeneous and photochemical reactions take place. A scheme of these various processes is shown in Figure 1.1.

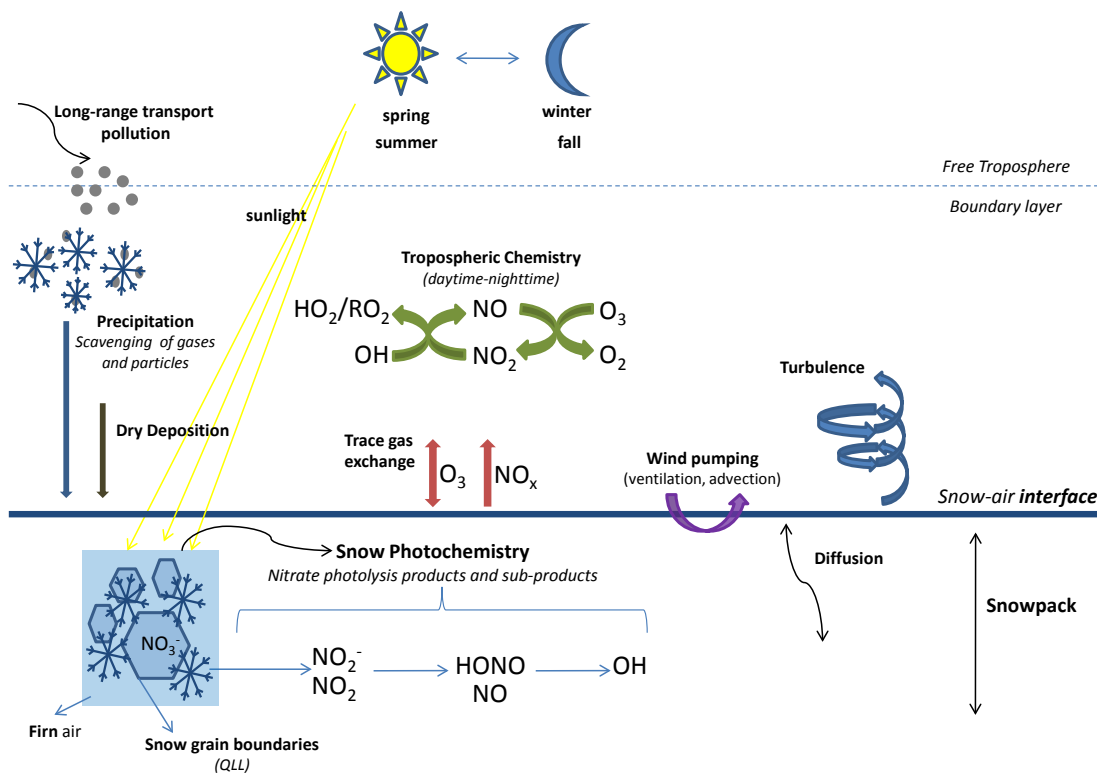


Figure 1.1. Physical and chemical processes involved in snowpack photochemistry at polar regions.

Nevertheless, many mechanisms are still not clearly understood, particularly the microphysical location of reactive species (particle phase, dissolved in ice or adsorbed on ice). Laboratory work suggest the existence of a quasi-liquid layer (QLL) (21–24) where gases might be dissolved and chemical reactions might occur, however more laboratory experiments and molecular dynamics studies are needed in order to quantitatively understand these processes.

Reviews of snow photochemistry (25,26) have recognized the need of a quantitative understanding of the impact of air-snow interactions at global level. During winter, the Northern Hemisphere can reach up to 40% of snow-covered land, and climate trends in the Arctic are more pronounced than in any other area on Earth (27), highlighting the need to understand air-snow exchange processes to adequately predict the effect of future changes.

NO_x are the drivers for many of the snow chemistry processes affecting the oxidative capacity of the atmosphere above a snowpack. Previous work in Summit (Greenland) by Honrath et al. (8) demonstrated that NO_x and HONO emissions were indeed higher than HNO_3 deposition, implying some degree of export of NO_x from the Summit boundary layer and implications for the relationship between ice-core nitrate and background atmospheric HNO_3 . In order to characterize the variables controlling NO_x cycling at Summit, a two-year experiment was conducted to measure NO_x gradients continuously in and above the snow, as well as meteorological variables to calculate turbulence. This experiment was part of a big scale project that aims to determine differences in snow photochemistry at various locations, in order to parametrize air-snow interactions at a global scale.

The work presented in this thesis focuses exclusively on the behavior of nitrogen oxides within the snowpack at Summit, Greenland. The main research questions addressed are how seasonal changes affect the NO_x profile in the snowpack and what are the main factors driving the distribution of these species in the firn air. Particular questions that motivated this work are:

- What is the budget of NO_x within the snowpack at Summit?
- How do these gases at Summit vary seasonally?
- How are NO and NO_2 distributed within the snowpack at Summit?

- How are NO_x affected by the presence of O_3 within the snow?
- How do variables such as wind, incoming radiation and snowpack temperature influence NO_x production and distribution within the firn?

In order to respond these questions and characterize the NO_x budget, an automated system for sampling firn air was mounted in Summit during July of 2008 and was kept running until July of 2010. This sampling system was previously used to measure trace gases at an alpine site in Colorado (28) with excellent results. The use of this system at Summit allowed the recollection of continuous measurements of trace gases within the polar snowpack over an extended period of time, without permanent supervision. The results presented here constitute the largest data set of NO_x within the snowpack and will be a valuable input for models attempting to describe snow photochemistry and air-snow interactions.

2. BACKGROUND

This chapter presents a review of literature and introduces basic concepts that will support the discussion of results. Physical properties and particular characteristics of the snow at Summit are presented. Photochemistry at high latitudes and chemical processes relevant for snow photochemistry are discussed.

2.1 Transport mechanisms and physical properties of snow relevant to snow photochemistry

Snow is a porous medium with a high surface area, high permeability and is able to transmit light. These characteristics are directly involved in the efficiency of snow as a photochemical reactor and its capability of releasing chemical species to the atmosphere. Among the specific properties that affect snow photochemistry, porosity, specific surface area, thermal conductivity, permeability and light transmission are undoubtedly the most relevant (29). The diffusion of gases through the snow also depend on the tortuosity of the medium (i.e. the ratio of the path length in a porous medium over the direct path length) and the sorption of gases onto the snow crystals.

In polar ice sheets, specifically in cold and high altitude regions such as Summit, cold and strong winds create thick layers of snowpack during winter (wind pack), composed of small solid rounded grains; summer is characterized by much lower density layers. Values measured at Summit and similar polar regions are $\sim 0.34 \text{ g cm}^{-3}$ for snow density at the top 50 cm (30), specific surface area of $150\text{-}380 \text{ cm}^{-2} \text{ g}^{-1}$ (29), thermal conductivity of $0.15\text{-}0.20 \text{ W m}^{-1} \text{ K}^{-1}$ (31) and permeability of $5\text{-}30 \times 10^{-10} \text{ m}^2$ (29).

The transport of gases through the snowpack occurs by diffusion and advection. In a study of transport properties at Summit, Albert (30) defined diffusion as the slow transport process driven by gradients in concentration or temperature. In the same study, advection or ventilation was defined as the movement of interstitial air within the snowpack due to presence of pressure differentials from wind blowing over rough surface or by wind turbulence. Advective processes can effectively increase both the rate and physical extent to which air carrying chemical species contacts the snow grains, thus increasing the available surface area for chemical interaction. Permeability, defined as the proportional factor between pressure differentials and the air flow velocity, is the key transport parameter for ventilation. At Summit, permeability increases with depth in the top several meters (30). This increase is related to daily and seasonal changes in temperature which results in metamorphism in the snow crystals, leading to increased pore space and increased permeability, particularly in the top meters of the snowpack. Albert et al. (30) also measured diffusion of SF_6 , an inert gas, showing that under low wind conditions (3 m s^{-1}) the transport of the gas in the top 15 cm appears to be controlled by diffusion, while under strong winds (9 m s^{-1}) evidence of ventilation was observed.

2.2 Photochemistry at high latitudes

The availability of photons capable of causing photochemical reactions in the atmosphere is called *actinic flux*, and corresponds to the flux of photons with wavelengths that range between 290 nm and 700 nm, (i.e. UV plus visible spectral regions) integrated overall directions of incidence.

Many photochemical reactions are driven by ultraviolet (UV) radiation because these photons contain the energy needed to break chemical bonds, but at the same time, their energy is still low enough to penetrate the ozone layer. The UV radiation is divided in three ranges: UV-A, UV-B and UV-C. The UV-C radiation corresponds to wavelengths shorter than 290 nm and is completely absorbed by the ozone layer, thus is not relevant for tropospheric chemistry. UV-B and UV-A radiation correspond to the range 290 to 320 nm and 320 to 400 nm respectively, and together represent a critical spectral region for atmospheric and snowpack photochemistry. The UV-B

levels are highly dependent on the ozone column and the solar zenith angle (SZA), which determines the degree of light attenuation; in contrast, UV-A has a lower dependence on both factors. Relevant examples of UV-B absorbers are O_3 and $\text{NO}_{3(\text{aq})}^-$ and for UV-A absorbers are NO_2 , nitrous acid (HONO) and NO_2^- .

At high latitudes, the SZA is usually larger compared to midlatitudes, thus decreasing photolysis rates due to a larger attenuation of radiation. However, polar regions are covered by snow (which has a high albedo) and more than 90% of the light in the UV region is reflected. This effect counterbalances the less favorable SZA and is specially significant for UV-A absorbing species, and as a result diurnally-averaged spring-time photolysis rates at high latitudes are often comparable to mid-latitude values (26, 32).

Once radiation reaches the snowpack, the region close to the surface (top few centimeters of the snowpack) will cause either an increase or a decrease of the available radiation, dependent on the SZA. When sun is overhead ($\text{SZA} = 0^\circ$), the actinic flux is enhanced because direct light is converted into diffuse light. At larger SZA, the actinic flux is decreased as a result of the forward scattering of light by snow grains (33). Deeper in the snowpack, diffuse radiation decreases exponentially with distance, a concept known as the *e*-folding depth $\epsilon(\lambda)$ (34). The *e*-folding depth should be considered as the characteristic illumination depth of the snowpack, where the majority of the photochemical reactions occur, thus this region is also known as the “photic zone”. The general range for $\epsilon(\lambda)$ in the visible and UV is between 5 and 25 cm for most snowpacks (29).

2.3 The quasi-liquid layer

The concept of a quasi-liquid layer was first sketched by Faraday (35) and after more than a century, the physical properties of this liquid-like layer still remain poorly understood. The surface of snow/ice exhibits a thin liquid layer which is originated by an imbalance in surface energy, caused by molecules at the interface with air that only encounter bonding forces at one side. To return to the equilibrium condition, the system decreases its free energy by converting a layer of solid into liquid (36) causing the melting of the surface layer.

Surface liquid layers on ice play a substantial role in many aspects of atmospheric chemistry, including chemistry of polar stratospheric clouds, ozone depletion over sea-ice and photochemistry within snowpacks. Over sea-ice surfaces, the thin liquid layer can be referred as the *brine layer* and it corresponds to a layer in equilibrium with the ice matrix. The brine layer is formed as a consequence of the depression in the freezing-point of water caused by the addition of solutes over a specific range of temperature. In contrast, the *quasi-liquid layer* (QLL) pertains only to pure water ice (no impurities) and it refers to the disordered region where mobility is greater compared to the bulk of the ice. The QLL can be considered as a surface aspect of the bulk transition from solid to liquid and thus its thickness depends on temperature (37). In summary, the quasi-liquid layer and brine layer are conceptually distinct: the QLL exists in the absence of impurities.

In snow photochemistry, the QLL poses many questions, ranging from the role that it plays as a medium for (photo)chemical reactions to the control that exert on the release of species to the gas phase. Laboratory studies have shown that the NO_x levels released from nitrate-doped ice matrices are controlled by desorption from the ice layers at the surface of the snow crystal rather than by photolysis rates of nitrate ions (38–40). The size of the QLL is influenced by temperature and ionic strength. The QLL thickens with an increase in temperature and/or presence of impurities (22, 41). Kahan et al. (42) have also reported structural changes in the QLL by addition of acid species that would enhance hydrogen bondings in the liquid layer. To date, many studies have been done in order to characterize the size of the QLL, but discrepancies due to differences in the sensitivity of measurement techniques have reported quite different values ranging from few nanometers to 100 nm (42). Theoretical estimations of the volume of the QLL are usually included in modeling studies of snowpack chemical processes, but these calculations are a large source of uncertainty in many of these modeling approaches (21, 43–45).

The most relevant features of the existence of a liquid-layer over snow/ice are first, the possibility of extrapolating to relevant temperatures the already existent aqueous phase chemistry, and second, that chemical reactions are likely to be enhanced in aqueous phase compared to bulk ice (46) thanks to the small volume involved and thus high concentration of species. The former facilitates the interpretation and modeling

of chemical processes within the snowpack, while the latter will have implications for many compounds such as aromatic pollutants which are photodegraded in snow but whose lifetimes at the air-snow interface have not been clearly characterized (24, 47).

Finally, although the QLL can be successfully invoked for qualitative interpretation of chemical processes in the snow, there is no direct experimental evidence showing its role in chemical reactions on the ice surface, since it is currently impossible to distinguish between processes on the ice surface or in the QLL (29).

2.4 Reactive species in snow photochemistry

2.4.1 Nitrate

Nitrate (NO_3^-) is one of the dominant anions found in snow in both polar regions (48). Several studies in the last decade had identified nitrate photolysis as the source of NO_x emissions from the snowpack (13, 49). NO_3^- is formed in the atmosphere by NO_x oxidation via OH and O_3 . During formation of the snow and precipitation, diverse gaseous and particulate species (e.g. nitric acid (HNO_3)) are incorporated into the snow crystals. Like most other solutes, NO_3^- is expected to be excluded from the ice matrix during freezing; thus, photolysis of nitrate is most likely to occur in the quasi-liquid layer within the ice microstructure. This key assumption is the reason behind using aqueous chemistry reactions to explain the mechanism of NO_x production within the snow.

The absorption spectrum for nitrate is dominated by a strong $\pi \rightarrow \pi^*$ band at 200 nm and a weak $n \rightarrow \pi^*$ band around 302 nm (50) (UV-B), which is the most relevant for atmospheric chemistry processes. The photolysis of NO_3^- occurs via two major channels at illumination wavelengths above 290 nm (51):



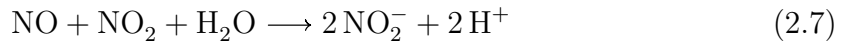
The rate of the first reaction exceeds the second roughly by a factor of 8 to 9 (39), thus the photolysis of NO_3^- could also represent a source of hydroxyl radicals in the firn air, which in turn can drive the oxidation of organic matter within snowpacks. The oxygen atoms produced in reaction 2.2 can react with oxygen to produce ozone and with nitrate to produce additional nitrite (NO_2^-) (43):



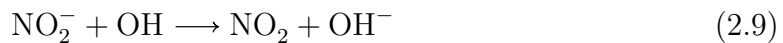
The absorption spectra of nitrite exhibits 2 bands at relevant wavelengths: 318 nm and 354 nm, both corresponding to $n \rightarrow \pi^*$ transitions; its maximum absorption is in the UV-A. Reaction 2.2 and 2.4 can be followed by photolysis of NO_2^- , which also can occur in a liquid environment as proposed by several laboratory studies (39, 40, 52):



thus nitrate photolysis in the QLL can generate NO as a secondary product. The oxide radical ion (O^-) produced is immediately protonated to yield OH radicals (53). Additional pathways for nitrite formation are reactions of NO with hydroxyl radical and NO_2 (43):



Nitrite can react with oxidants such as O_3 or OH producing a new route for NO_2 production (43):



Reactions 2.5 and 2.9 are the major sinks for nitrite on polar snow grains as found in a laboratory study by Chu and Anastasio (52), although they would not be a relevant source for OH (compared to other sources such as hydrogen peroxide photolysis) due to the low estimated concentrations of nitrite in snow grains.

2.4.2 Nitrogen oxides

Since emissions of NO_x to the gas phase and subsequently to the atmosphere depend on the residence time at their place of production, it is relevant to understand the fate of these species in the QLL and the possible pathways that they can go through before being released to the firn air.

The main product from nitrate photolysis is NO_2 (Reaction 2.1). NO_2 is not a highly soluble species (Henry's Law constant on the order of $10^{-2} \text{ mol L}^{-1} \text{ atm}^{-1}$ (54)), which suggest that once formed it would rapidly be volatilized to the gas phase. However, laboratory studies (38,39,55) suggest that only the NO_2 produced closest to the interface with the firn air is able to escape to the gas phase, while the remainder is trapped and undergoes secondary photolysis to produce NO (Reaction 2.10). Also, Boxe et al. (55) proposed that hydrolytic disproportionation of the photogenerated NO_2 into NO_3^- and NO_2^- would be the dominant dark loss pathway for the trapped NO_2 .

It has also been suggested (43) that a relevant sink for nitrogen dioxide is the oxidation back to NO_3^- by the OH radical before being released to the gas phase, pathway that can reduce NO_3^- destruction rate by 40%. Currently, new modelling studies suggest that the concentration of OH in the QLL remain too low to oxidize NO_x in the QLL (56).

Jacobi and Hilker (43) also suggest that NO concentrations in the QLL are rather small and that probably most of the NO measured in snow experiments (13) must be the product of gas phase reactions such as NO_2 or HONO photolysis. Other experiments have ruled out the production of NO from NO_2 photolysis due to faster diffusion of NO_2 to the gas phase compared to its photolytic lifetime under the modeled conditions, therefore the contribution (if any) to NO production via Reaction 2.10 in the QLL has not been taken into account in current modeling approaches (21).



2.4.3 Nitrous acid

Another important secondary product from NO_3^- photolysis is nitrous acid (HONO). Nitrous acid fluxes have been measured in many field campaigns, but the mechanism of formation within the snow is still unclear (26). In the QLL, the chemistry of oxidized nitrogen depends strongly on the pH, which determines the acid-base equilibrium of the species. The pKa of HONO is 3.25 at 25°C and the Henry's law constant is $49 \pm 3 \text{ M atm}^{-1}$ (57). Anastasio and Chu (58) found that at pH 2, the photoformed nitrite from Reaction 2.2 rapidly equilibrates between HONO and H_2ONO^+ (nitrous acidium ion), with HONO being the dominant form in the pH range between 2 and 3. HONO formed in the QLL has two major pathways: photolysis or evaporation, and both are observed in almost equal proportion across a wide range of values (pH 0.5 to 4). The importance of pH as a controlling factor in HONO emissions has been suggested as extremely relevant since laboratory measurements have found that acidic snow will most likely release HONO and alkaline snow will rather retain nitrite and HONO emissions will not be observed (59). This has been supported by the fact that HONO has not been detected in places with alkaline snow (12).

A second factor in determining whether HONO is a relevant species in the QLL is the mass transport of HONO to the gas phase. Jacobi and Hilker (43) determined that its transfer rate is significantly smaller than NO_x , based on Henry's law constants and the greater solubility of HONO in aqueous phase, a result also supported by Pinzer et al. (60). In addition, since Reaction 2.2 is much slower compared to reaction 2.1, the concentration of NO_2^- (and thus the concentration of HONO) would be negligible in the QLL. Therefore, the observed HONO emissions to the atmosphere might originate from gas phase reactions in the firn air probably by Reaction 2.6. A heterogeneous reaction of NO_2 with light absorbing organic compounds at the snow surface crystal has been proposed as an alternative explanation to the presence of HONO in the firn air (12, 43, 59, 61), as well as a 'dark' mechanism involving protonated nitrosamide (NH_3NO^+) under alkaline conditions (62). In summary, the remaining question is whether HONO is actually formed on the snow grain surface or whether it is formed in the firn air following to the release of NO and OH.

2.5 Halogens

The influence of halogens in polar chemistry is mostly known by the existence of ODEs (Ozone Depletion Events) during springtime both in the stratosphere and troposphere. In the troposphere, the source of these events is most likely the reactive bromine species released from sea salt via photochemical and heterogeneous reactions, known as the 'bromine explosion' (63). Although the presence of halogens in snow is more common in coastal locations, several measurements of bromide and methyl halides have been made at Summit (11, 64). Dibb et al.(64) observed a summer correlation between ^{210}Pb (which can be used as a tracer for vertical transport from the free troposphere to the boundary layer) and Br^- . The results suggested that the presence of small amounts of bromide in snow and firn air are due to intrusions of free tropospheric air masses that have been in the Arctic basin during ODEs, creating a pool of bromide that is not efficiently transported inland until summer.

Although the role of halogens within the snow (away from coastal sources) is not completely clear, there are many hypotheses that link their presence with perturbations of the NO_x and HO_x cycles, with the observed ozone depletion (65) and gaseous elemental mercury (GEM) depletion (66) both within the snowpack. The latest modeling studies coupling snowpack-atmosphere chemistry have included reactive bromine cycling through oxidation of bromide to Br_2 in the QLL with subsequent release of molecular bromine to the interstitial air in a process that depends on OH radical concentration in the QLL (44).

2.6 Ozone

While ozone in the polar boundary layer depends either on meteorological conditions that result in local production (e.g. South Pole, (67)) or transport of stratospheric air masses and exchange with the troposphere (e.g. Summit (7)), several studies have observed ozone destruction in the snowpack under both irradiated and dark conditions (65,68,69). At Summit, ozone depletion rates increased significantly with seasonal and diurnal cycles of sunlight causing marked gradients between the atmosphere and the snow, resulting in uptake of ozone to the snowpack that depends

strongly on irradiance and wind pumping (69). At Alert, chamber experiments under dark conditions resulted in short O_3 lifetimes indicating destruction at least within the first 10 cm of the snowpack (68). Between the mechanisms proposed to explain ozone depletion, halogen (e.g. bromine) chemistry is the most popular. Reactions similar to the mechanism involved in ODEs in the Arctic boundary layer would be able to destroy O_3 fast enough to explain the destruction rates observed at Summit:



Since Br^- concentrations reported at Summit (64) are too low to explain the magnitude of the ozone depletion, other mechanisms have been invoked. Black carbon, traces of crustal material, humic and fulvic acids (68), hydroxyl radicals and unsaturated hydrocarbons (69) are all different species that can react with ozone. However, none of the mechanisms can totally explain the loss of ozone in the snowpack, therefore another unidentified photochemically generated sink must be present to explain the observed ozone destruction rates.

2.7 HO_X

The HO_X family consist of OH plus HO_2 radicals. The main source of OH radicals at high latitudes is the photolysis of hydrogen peroxide (H_2O_2) (Reaction 2.14) (70). (H_2O_2) is one of the major oxidants involved in snow photochemistry and probably one of the most common species found in snow. H_2O_2 is thermally cycled between atmosphere and snowpack, with emissions during daytime and deposition at night when temperatures decrease. Another important source of HO_X is formaldehyde (CH_2O), also thermally recycled between near-surface snow and the atmosphere (Reaction 2.15) (26):





One of the main sinks of OH radicals within the snow is the oxidation of organic compounds, releasing smaller volatile organic compounds such as formaldehyde, which is also one of the most abundant identified Volatile Organic Compounds (VOCs) from polar snow (71, 72). The reaction of OH with organic compounds in the condensed phase generally produces HO₂ which could eventually regenerate H₂O₂. Current mechanistic studies of NO₃⁻ photolysis in the QLL have added reactions including both H₂O₂ and HCHO (considered as the main OH source and sink, respectively) to include HO_x chemistry. The addition of these reactions improved significantly the representation of observed laboratory measurements (56) and demonstrated the relevance of these species on nitrate photolysis.



2.8 Implications of snowpack photochemistry

Nitrogen oxides are one of the key drivers in atmospheric chemistry, controlling the oxidative capacity of the atmosphere through ozone production/destruction. The process that releases nitrogen oxides to the snowpack also releases many other radicals of relevance for atmospheric chemistry. In remote areas, particularly in polar regions, the existence of a photochemically driven source such as snowpack emissions can impact the local boundary layer chemistry. In Antarctica, where very stable meteorological conditions favor the presence of a shallow boundary layer, reported NO values are one or two orders of magnitude higher compared to other polar sites (14). These high NO_x values cause an enhancement of O₃ production in the lower several hundred meters of the boundary layer (67). On the other hand, the production mechanism of NO_x also involves the release of OH radicals, which can oxidize organic matter present in snow to low molecular weight carbonyl compounds (73). Indeed, emissions of formaldehyde (HCHO) and acetone (CH₃CHO) have been reported (9, 17, 72) in many polar sites.

NO_x production from nitrate photolysis within the snowpack is also relevant to paleoclimatic studies. The interpretation of nitrate isotopes in ice-cores has been widely used to track back the oxidative state of the atmosphere. Nitrate is formed in the atmosphere by oxidation of nitrogen oxides with O_3 or OH radical, and each pathway has a particular isotopic signature that can trace changes in the oxidative characteristics of the atmosphere. Post-depositional losses of nitrate due to photolytic processes can alter the historical record by isotopic fractionation (74), complicating the reconstruction of past atmospheric conditions. This is specially observed at locations with low annual accumulation rates, such as Antarctica (75–77). Records of H_2O_2 are also in risk of being perturbed, since hydrogen peroxide constitutes the most likely source for OH radicals after photolysis.

Therefore, the understanding of snowpack photochemistry processes is essential to adequately reconstruct past atmospheric conditions as well as to improve our knowledge on current boundary layer chemistry above snow-covered surfaces. After qualitative and quantitative description of this system, it will be possible to correctly parametrize these air-snow interactions and include them in global models, in order to predict possible effects due to variations in snow-covered areas.

3. RESEARCH DESIGN AND METHODS

This research project was a collaboration between Michigan Technological University (MTU) and the Institute of Arctic and Alpine Research (INSTAAR), University of Colorado. Nitrogen oxides as well as total reactive nitrogen measurements were made by MTU, while ozone and meteorological measurements were made by INSTAAR. Wind, temperature and radiation data are here used as ancillary measurements with permission of INSTAAR. Measurements at Summit, Greenland started on June 2008 and were carried out continuously until July 2010.

3.1 Site Description

The measurements were carried out at Summit Station, located at the peak of the Greenland ice cap at $72^{\circ}35'46.4''\text{N}$ $38^{\circ}25'19.1''\text{W}$, 3200 m elevation from mean sea level, and nearly 400 km inland (see Figure 3.1). Summit is the only high altitude observatory at the Arctic Circle operated year-round offering access to the free troposphere and relatively free of local influence. The high elevation provides extreme cold temperatures and low water vapor mixing ratios, and combined with a high snow accumulation rate and a strong seasonal radiation cycle makes Summit a unique polar site to study photochemical cycling of reactive species in the snow.

The experimental site was located 0.8 km away from camp in the 'Clean Air Zone', which is located South from main camp. Except for special circumstances, access to the area is strictly prohibited, including foot and vehicle traffic. Prevailing winds are from the south for at least 80% of the year, facilitating identification of pollution events from the main camp.

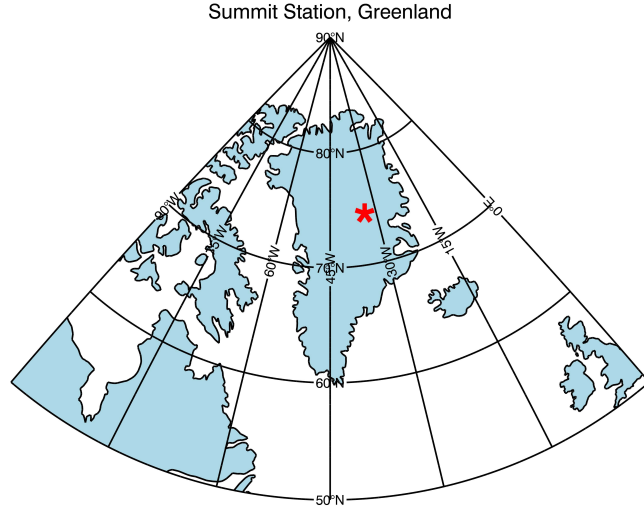


Figure 3.1. Geographical location of Summit Station

3.2 Experimental Setup

The experimental setup comprises a 10 m tower, hereafter Met Tower, and a multi inlet 2.5 m small tower, hereafter Snow Tower. Both towers were equipped for meteorological and chemical measurements and connected to an underground heated, insulated facility. The Flux Facility was located downwind from both towers during clean-sector flow and housed calibration gases, instrumentation and data acquisition systems. A picture of the experiment site after the installation is shown at the top of Figure 3.2 and a detailed schematic of the site is included in Appendix A (see Figure A.1). The towers were installed in summer 2008 and snow was allowed to accumulate around them during the two years of experiment, which was particularly relevant for the snowpack measurements. Periodic maintenance (cleaning rime and measurement of the distance between instruments and snow surface) was performed weekly during the summer season and monthly over the winter season. For periodic access to the Met Tower and Snow Tower area, as well as for any other maintenance or repair of instruments, a flag-delimited walk path (located downwind from the towers

during clean-sector flow) was established in order to avoid further disturbance of the snowpack. Other than during these periodic maintenance events, which were logged into a field notebook file, the snowpack was essentially undisturbed.

3.2.1 Met-tower

The Met-tower (Figure 3.2b) was a 10 m tower equipped with meteorological instruments capable of monitoring boundary layer variables such as wind speed and wind direction, temperature and turbulence parameters at different heights, in the time scale needed to calculate ozone fluxes using the eddy correlation technique, as well as for measuring ozone and nitrogen oxides gradients simultaneously. A detailed schematic of the instrumental arrangement (Figure A.1) along with a brief description of each of the meteorological instruments can be found in the Appendices section.

The Met-tower also supported the main inlet box for both the nitrogen oxide (NO_x) and total reactive nitrogen (NO_y) instruments (see Figure A.1). The NO_x inlet box, located at the bottom section of the tower, has two inlets for NO_x measurements. The top inlet was used as reference to determine the enhancements of NO_x mixing ratios within the snowpack.

3.2.2 Snow-tower

The snow-tower (Figure 3.2c) was made of square aluminum alloy (3.8×3.8 cm) tubing with eight 60 cm long cross bars (1.3×1.3 cm) separated by 30 cm between them, similar to the tower used by Seok et al. (28). In each cross bar a pair of sampling inlets was installed, and to avoid debris or snow from entering the sampling line, the inlets were fitted with syringe filters (25 mm Acrodisc[®] hydrophobic polytetrafluoroethylene (PTFE), Pall Life Sciences, Ann Arbor, MI, USA).

The snow-tower was located approximately 10 m east and parallel to the met-tower. When the snow-tower was installed, four inlets were buried in the snowpack at depths of 1.1, 0.8, 0.5 and 0.2 m from the snow surface. Inlets above the surface, located at heights of 0.1, 0.4, 0.7 and 1 m, were gradually covered by snow which allowed to sample from a 'natural' snowpack. At the end of summer 2009 an extension with 6 additional inlets was installed on the snow-tower.

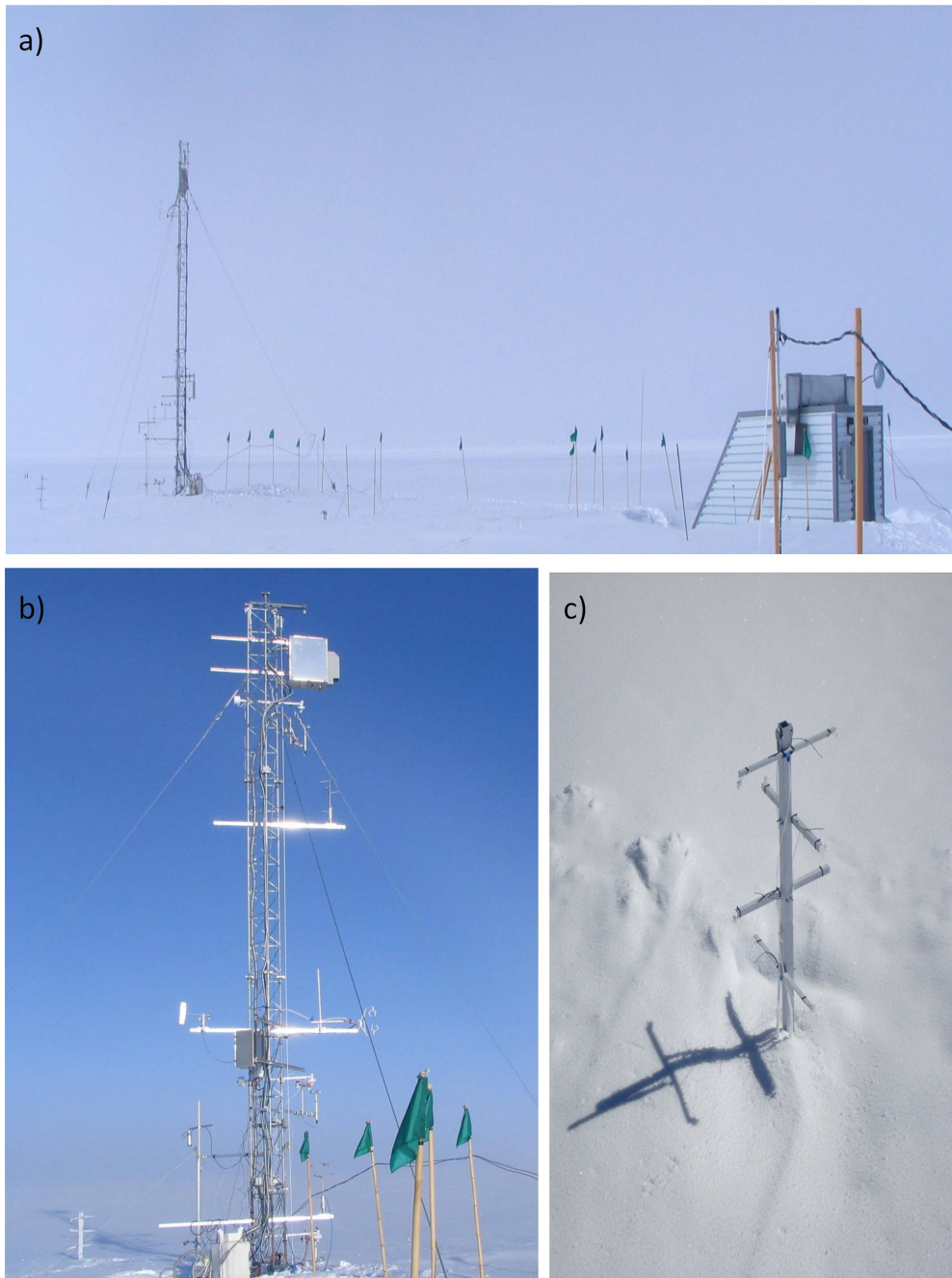


Figure 3.2. Experimental Setup after installation in 2008. **a)** View of the experimental site with both towers and the entrance to the Flux Facility. **b)** Met-tower. At the bottom left corner is possible to appreciate the snow-tower. **c)** Snow-tower.

Knowledge of the location of each sampling inlet within the snow is extremely relevant to characterize the chemical behavior of the snowpack. The depth of each sampling inlet relative to the surface changes after each snowfall event or by accumulation of snow due to blowing wind. The variation in the depth of each inlet was periodically monitored by measuring the distance between the top inlet and the surface of the snowpack. Then, since the distance between each cross arm is known, is possible to calculate the distance relative to the surface of the snowpack for each of the sampling inlets.

The snow-tower sampling lines were all perfluoroalkoxy (PFA) Teflon[®], inner diameter of 3.9 mm and outer diameter of 6.4 mm, with approximately equal length (38 m). The sampling lines along the entire section outside of the Flux Facility were covered with pipe insulation and a self-controlling water pipe heater was installed. The heater helped to maintain the sampling lines temperature above 0°C to prevent water from freezing and clogging the sampling lines. The pipe insulation containing the sampling lines was protected by a ~11 cm polyvinylchloride (PVC) pipe which was in turn located in a larger 28 m aluminum spiral lockseam jacket conduit of ~55 cm in diameter, called the Arctic Pipe (see Figure A.1, which also hosted 3 more PVC pipes with lines, power and data cables from the Met Tower. The function of the Arctic Pipe was to carry all the lines and cables from both towers to the underground facility. To protect lines and cables, the Arctic Pipe was filled with polyurethane foam insulation and heated at a set point of -6.5°C.

3.3 Sampling Technique

Solenoid valves were used to select between sampling inlets and were controlled by digital input/output modules and Labview software (National Instruments, Austin, Texas, USA), through the INSTAAR computer system.

Air was sampled at a rate of ~2 standard liters per minute (slpm) and split between two inlets at each sampling level, thus the effective sampling rate per inlet was ~1 slpm. Sampling interstitial air in the snowpack disturbs the natural air transport which can generate artifacts in the measurements (29, 68). The measurement technique used here alternated sampling between levels every 10 minutes, sampling

a volume equivalent to the air contained in a sphere of radius ~ 15 cm at each level. The separation between each cross arm holding the inlets was 30 cm, therefore the overlap between sampling inlets was minimum. To estimate the time needed for this volume of air to re-equilibrate to its original condition, the approach of Seok et al. and Bowling et al.(28, 78) was followed. Considering the diffusion coefficient for SF_6 ($0.06 \text{ cm}^2/\text{s}$) as an upper boundary for chemical species diffusing through snow at Summit (30), the estimated time for reaching a steady-state condition would be ~ 65 min. This is faster than the length of the complete sampling cycle (8 inlets = 80 minutes, and after the extension, 14 levels = 140 minutes), allowing the assumption that the advective influence of the sampling was negligible. This assumption was further tested by experiments where the sampling cycle was reversed or modified, and where the sampling intervals were decreased. In all the experiments the concentrations did not changed significantly between sampling events at the same level, showing that the data obtained was representative of the real conditions within the snow at each depth.

3.4 Measurement Technique

The instrument used to measure NO_x is a modification of the MTU $\text{NO}/\text{NO}_2/\text{NO}_y$ instrument described in detail by Peterson et al.(79) and Peterson and Honrath (80), where the features needed to determine NO_y have been removed. Thus, only a brief overview of the measurement technique will be given here.

3.4.1 Measurement Cycle

The measurement cycle included seven modes: NO/Z , NO_1/M , NO_{x1}/M , NO_{x2}/M , NO_2/M , $\text{NO}_{\text{snow}}/\text{M}$, $\text{NO}_{x\text{snow}}/\text{M}$. Each mode had a duration of 86 seconds and the total length of the cycle was 10 minutes. The measurement cycle (and instrument functions in general) was controlled by Labview software. Voltage signals are sent and/or received and interpreted by the software to control pressure sensors, temperature and mass flow controllers, solenoid valves and AC/DC suppliers.

The first mode (NO/Z) corresponds to the zero mode where zero air is measured to determine the background signal of the photomultiplier (PMT) tube due to thermal

noise, dark pulses and other chemiluminescent reactions. The zero level is determined by redirecting the O_3 flow into a zeroing volume in order to produce the reaction between NO and O_3 out of the view of the PMT. A flow diagram of the Zeroing mode is included in Appendix A.

The NO/M and NO $x_{1,2}$ /M modes correspond to the actual measurement of NO and NO $_x$ for ambient and snowpack, with the NO $_2$ converter in the Off position (NO/M) or switched On (NO x /M). The number 1 and 2 indicate measurements at Inlet 1 or Inlet 2, both above the surface. Inlet 1 corresponds to the inlet located at the inlet box on the Met Tower and Inlet 2 corresponds to the inlet located in the lower arm of the tower (see Figure A.1). The measurements in the snow modes correspond to the specific inlet of the Snow Tower that is being sampled; the switch from ambient air to snowpack air sampling is controlled by a solenoid valve located in the Inlet Drawer of the NO $_x$ instrument. A flow diagram of the measurement modes is included in Appendix A.

Each measurement mode was recorded as an average of the last 30 seconds of each mode. For the snowpack measurements, this implies 30-sec averages for the NO $_{snow}$ /M and NO x_{snow} /M every 10 minutes, and measurements at the same level of the snow-tower every 80 minutes (or 140 minutes after the extension). Measurements were further averaged hourly or daily for posterior data analysis.

3.4.2 NO measurement

NO was determined using ozone chemiluminescence. Air was sampled at a flow rate of 550 standard cubic centimeters per minute (sccpm) and mixed with 200 sccpm O_3 in O_2 ($\sim 4\%$ per volume) at approximately $-7^\circ C$ in a low pressure (5-7 torr) reaction chamber. The chemiluminiscent excited-state NO $_2^*$ is formed as a product of the reaction between NO and O_3 . The decay of NO $_2^*$ results in emission of light, and the emitted photons are detected by a red-sensitive photomultiplier tube (81). The ozone required for this reaction was generated by applying a high voltage discharge to an O_2 (Welding grade, Airgas, Radnor, PA, USA) flow of 200 sccpm.

Instrument sensitivity is determined using standard addition of 0.8 ppmv NO (Scott-Marrin, Inc., Riverside, CA, USA) in N_2 (Standard grade, Airgas, Radnor,

PA, USA). The sensitivity to NO is calculated as follows:

$$S_{\text{NO}} = \frac{\text{NO/C} - \text{NO/M}}{[\text{NO}]_{\text{cal}}} \quad (3.1)$$

where NO/C corresponds to the PMT signal in counts per second (cps) due to standard addition of NO during calibration, NO/M corresponds to the PMT signal due to actual NO (cps) and $[\text{NO}]_{\text{cal}}$ corresponds to the mixing ratio of the NO calibration gas in pptv. NO mixing ratios were determined from the difference between photon count rates during the measurement mode and zero modes and the sensitivity, as described by Equation 3.2

$$[\text{NO}] = \frac{\text{NO/M} - \text{NO/Z}}{S_{\text{NO}}} \quad (3.2)$$

Corrections to sensitivity due to reaction of ambient O_3 and NO within the sample line during calibrations are detailed in section 3.5.1.

3.4.3 NO_2 measurement

NO_2 was detected as NO following conversion in a NO_2 photolytic converter (Air Quality Design, Inc., Wheatridge, CO, USA) with an UV-LED array (λ ca. 380-410 nm). The average conversion efficiency, given by Equation 3.3 was $\sim 50\%$. The derivation of sensitivity and mixing ratios for NO_2 are given in Appendix B.

$$\text{NOxNO2Cnv} = 1 - \frac{\text{NO}_X/\text{C} - \text{NO}_X/\text{C}/\text{UV}}{\text{NO}/\text{C} - \text{NO}/\text{C}/\text{UV}} \quad (3.3)$$

3.4.4 Uncertainties of NO/ NO_2 measurements

The uncertainties of NO and NO_2 measurements are determined by the measurement accuracy, precision and artifact corrections. Measurement precision and uncertainty in the artifacts correction were the main factors affecting total uncertainty at low mixing ratios. At high mixing ratios, measurement accuracy is the primary source of uncertainty (79).

The accuracy of the measurements was estimated to be a 2.1% based on the total uncertainty of the sample and calibration mass flow controllers and the NO standard calibration gas mixing ratio. Precision of each measurement was related to counting noise, which resulted from photon counting statistics. Each measurement was recorded as 30 seconds average and then compared to the expected Poisson value from counting statistics. Values with standard errors greater than 3 times the Poisson value were removed during data reduction. These measurements were more likely affected by pollution from camp or by occasional electronic noise spikes. After this previous data screening, two-sigma precision of individual 30 seconds average for NO and NO₂ measurements was estimated to be less than 3 pptv.

Artifacts are mainly caused by chemiluminescent reactions of O₃ with the walls of the reaction chamber as well as interferences from alkenes. To avoid potential bias in the measurements due to interferences, artifact tests for both NO and NO₂ were done in zero air (Breathing air grade, Airgas, Radnor, PA, USA) three times per week, for the NO/Z, NO/M and NO_X modes. The NO artifact was in the range of 3 to 5 pptv and for NO₂ between 5 and 10 pptv.

3.4.5 Calibration

Calibrations were performed twice-daily by standard addition of NO gas to the sample flow. During calibration mode, NO₂ is formed via titration of NO with O₃ using a low pressure mercury lamp (BHK Inc., Ontario, CA, USA) to generate O₃. The instrument calibration parameters include NO and NO₂ sensitivities, zeroing efficiency, and NO₂ conversion efficiency. Some of these parameters were already presented and the derivation of the NO₂ sensitivity is given in the Appendix B.

The calibration cycle included six modes and the length was 30 minutes. To ensure that each mode has reached equilibrium, only the last 20 seconds of cps data were used to calculate the calibration parameters. Polluted or incomplete calibrations (calibrations that were aborted before finishing) were not considered. If a calibration is deleted, the values are interpolated from the calibration before and after.

Calibrations were performed at the ambient reference inlet (top inlet at Met-tower). Corrections due to differences in residence time within the snow-tower sampling lines are detailed in section 3.5.1.

3.5 Data Analysis

3.5.1 NO_x measurements correction

Sampling lines used in the experiment were ~ 60 ft (snowtower measurements) and ~ 100 ft (ambient measurements) long. The residence time of the sample in each of the tubings was calculated using tubing dimensions and purge flow adjusted to standard conditions of temperature and pressure, resulting in ~ 15 s and ~ 33 s for the snowtower samples and ambient samples, respectively. During the transport through the tubing, NO will react with ozone in the sample air, according to the reaction



which has a rate constant $k = 1.2 \times 10^{-14} \text{ cm}^3 \text{ molecule}^{-1} \text{ s}^{-1}$ at $T = 0^\circ\text{C}$ (82). Since the sampling tubes are protected from light, NO re-conversion due to NO₂ photolysis can be neglected and reaction 3.4 will lead to partial conversion of NO to NO₂, resulting in a systematic error that will underestimate NO and overestimate NO₂. The magnitude of this error will depend on O₃ and NO concentrations as well as on variations in flow that would alter the residence time of the gases in the sampling tube. The flow was fairly steady through the whole experiment, with 550 sccpm for ambient measurements and 1250 sccpm for snowtower measurements. Slight variations in flow at the snowtower lines were detected due to ice blockage within the lines, but these variations affected mainly the levels above the snowpack and were not taken into account at this point. Under average summer conditions at Summit, where ambient O₃ is usually in the order of 40-50 ppbv and NO is in the order of 20-50 pptv, the loss of NO due to reaction with O₃ was estimated on 30-40% for ambient measurements and 15-20% for the snowtower measurements.

For the ambient measurements, this error is taken into account during the calibrations by injecting the NO calibration gas at the inlet, and therefore any losses are considered in the calculation of the mixing ratios at the calibration inlet. All the other measurements at the snowtower inlets as well as at the bottom inlet of the Met-tower

will be affected by the difference in flow (and thus in residence time) and/or by the difference in O_3 concentrations between the level at which calibrations are performed (~ 3 m above surface) and the level where the measurements are taken.

The procedure to correct the snowtower data involved two steps. First, it was necessary to correct the observed sensitivities to NO. During calibrations performed with zero air, i.e. no ozone present, the sensitivity value obtained was in average 6.5 cps ppt^{-1} . But during calibrations performed with ambient air, the sensitivity dropped to values ranging between 3.5 to 4 cps ppt^{-1} . This decrease in the sensitivity was attributed to the loss of NO calibration gas due to reaction with ambient O_3 along the sampling line. In order to correct for this effect, it is necessary to calculate the sensitivities considering zero losses due to reaction with ozone under the flow and ozone conditions corresponding to the inlet where calibrations are performed. This was done by selecting periods where NO sensitivity and ambient O_3 were clearly anti-correlated, i.e. increases in ambient ozone can be related to a decrease in sensitivity. A linear fit analysis of these periods was performed according to the equation:

$$\ln SNO = \ln SNO_o - k t [O_3] \quad (3.5)$$

where $\ln SNO$ is the natural logarithm of the observed sensitivity to NO, k is the rate constant for reaction 3.4, t is the residence time in the sampling line and $[O_3]$ the ozone concentration at the time of the calibration. The derivation of equation 3.5 is presented in Appendix B. The intercept of the linear equation ($\ln SNO_o$) represents the natural logarithm of the sensitivity to NO in the absence of O_3 and therefore the intercept values obtained by doing the linear fit must be close to the value of the sensitivity calculated during calibrations performed using zero air (SZA). On the other hand, the slope of the linear fit must be close to the value of the rate constant of reaction 3.4. A correlation plot of $\ln SNO$ versus $[O_3] \times t$ for one of the periods where both sensitivity and O_3 were anti-correlated is showed in Figure 3.3.

This correction produced a change in the values of sensitivity, increasing from an average of $4.3 \pm 0.35 \text{ cps ppt}^{-1}$ to an average of $6.1 \pm 0.45 \text{ cps ppt}^{-1}$, which is closest to the average of 6.5 ± 0.25 of the sensitivities calculated using zero air. A time-serie plot of all the sensitivities (non-corrected, corrected, and zero air) is presented in Figure 3.4. The variability observed in the corrected values must be attributed to

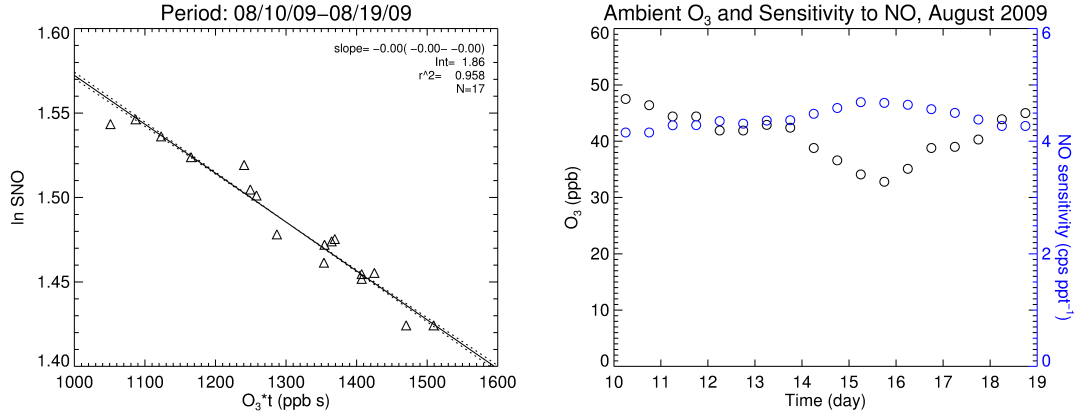


Figure 3.3. Correlation plot and time series of one of the periods selected for correcting sensitivity.

instrumental effects that could not be clearly identified.

The second step in the snowtower data correction included the calculation of the 'real' NO mixing ratios (or mixing ratios at the inlet) using the mixing ratio detected by the instrument and considering the O_3 losses through each of the lines. This was done by determining the O_3 mixing ratio at the time of the NO measurement and using the integrated rate law equation for reaction 3.4:

$$[NO] = [NO]_o \times \exp^{-k \cdot t [O_3]} \quad (3.6)$$

where $[NO]$ is the detected mixing ratio, k is the rate constant for reaction 3.4, t is the residence time in the sampling line, $[O_3]$ is the O_3 mixing ratio at the time of the measurement and $[NO]_o$ is the NO mixing ratio at the inlet, before any loss due to O_3 . $[NO]_o$ is the final mixing ratio used for this work.

The degree at which this correction affected the original NO values for levels within the snowpack is showed in Figure 3.5. Differences ranged from less than 10 pptv at the bottom level to ~ 30 pptv at the levels where NO is at its highest magnitude. There are two main factors that influence the relevance of this correction. First, the difference between original and final NO mixing ratios is greater in those levels where NO mixing ratios are higher, i.e. inlets 5, 6 and 7 that represent depths of 20-80 cm during spring-summer 2009. Second, the difference between original and final NO values increases during summer months, when O_3 is depleted within the

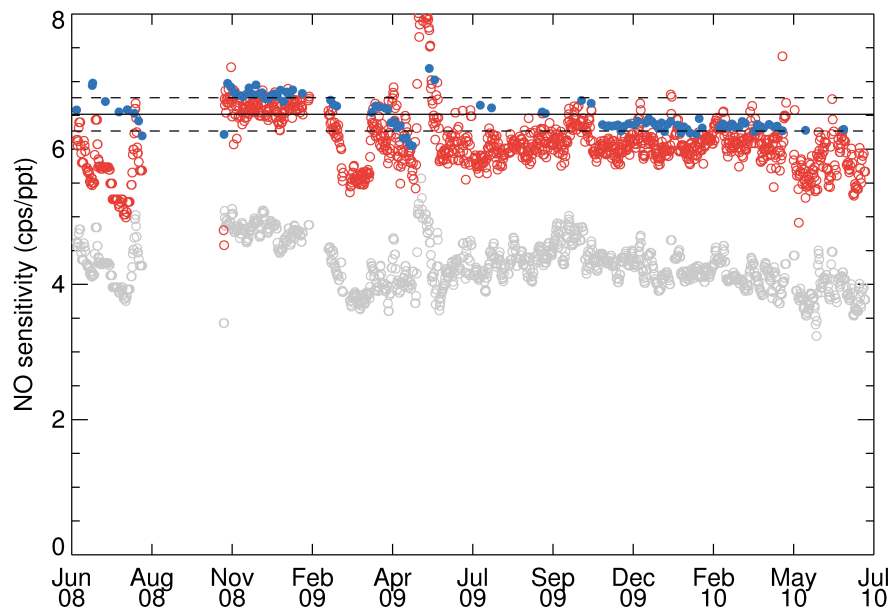


Figure 3.4. Time series of NO sensitivity. Observed sensitivities are plotted in grey, SZA are plotted in blue and corrected sensitivities are plotted in red. Solid line represents mean of SZA and dashed lines represent \pm SD of SZA.

snow. O_3 depletion within the snowpack increases the difference respect to ambient values, which are the values considered during the calibrations. In other words, if the O_3 magnitude within the snowpack is far from the ambient O_3 values at the calibration times, the correction applied will have more relevance in determining the final NO mixing ratios. The levels above the snow are not shown since the correction is not relevant for levels with O_3 concentrations similar to ambient, except for inlet 9, located right above the surface of the snowpack, where the correction becomes relevant at summer time. Finally, since NO_x mixing ratios are not influenced by NO to NO_2 conversion, it is possible to assume that NO_x values remain constant after the correction presented here, allowing to determine NO_2 mixing ratios at the inlet by subtracting the corrected NO mixing ratios from the NO_x values.

3.5.2 Data Screening

To remove possible impact from NO_x emissions from Summit camp, the measurements taken during North winds were excluded from the final data set, representing 5% of the total data base. Thus, the results presented in this work include only observations obtained during Clean Air flow, which corresponds to the area between 60 and 300 degrees (ENE-WNW).

In addition, measurements taken during times where the pressure at the reaction vessel was below 2 torr were also eliminated from the final database in order to assure a reliable measurement. Low pressure within the reaction vessel was usually caused by ice blockages in the sampling lines.

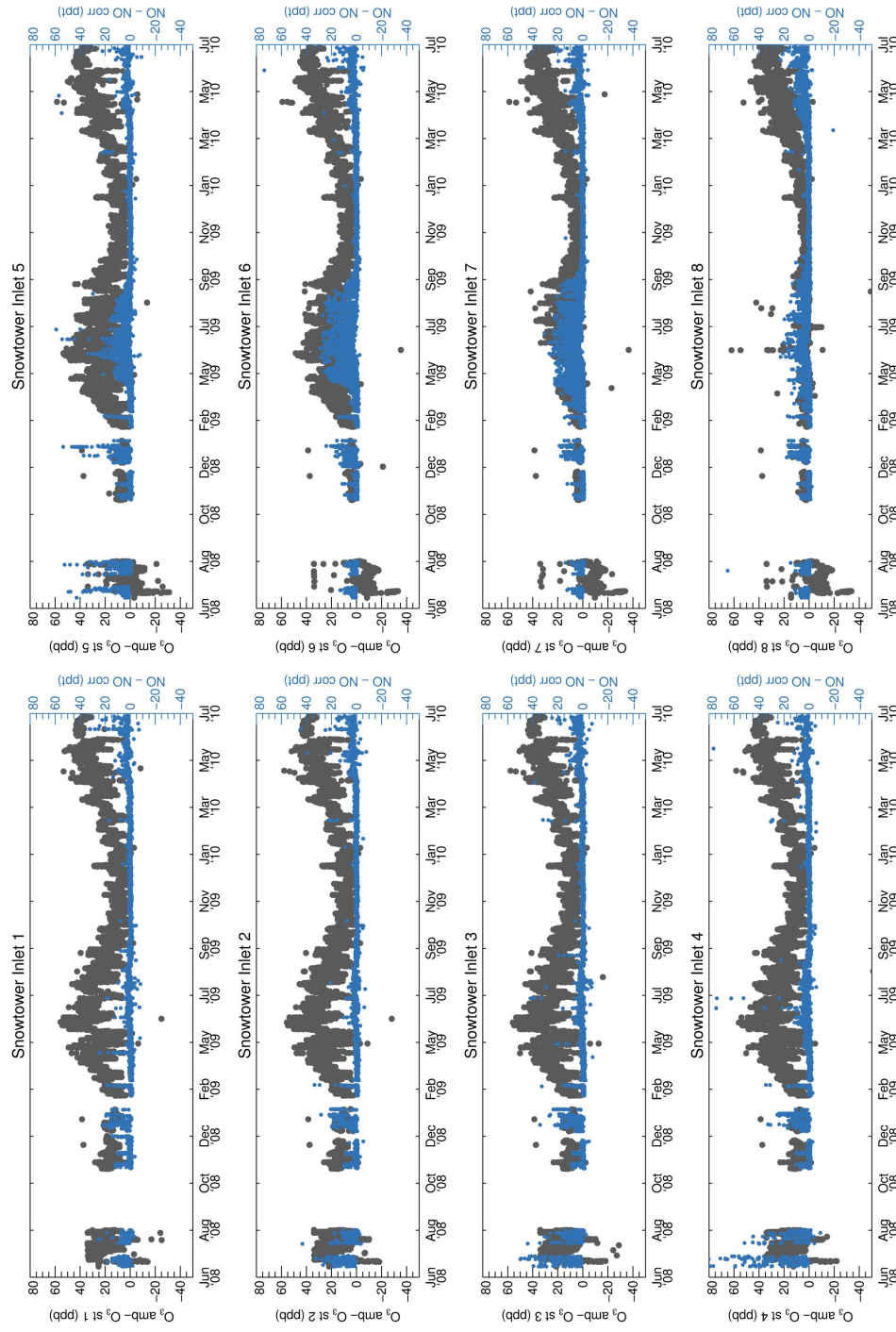


Figure 3.5. Magnitude of NO correction at different levels within the snow. NO difference between non-corrected and corrected mixing ratios is showed in blue. Difference between ambient and snowpack ozone is plotted in dark grey. Inlet 1 is the deepest level in the snowpack.

3.6 Ancillary measurements

3.6.1 Ozone

Ozone measurements within the snowpack (by INSTAAR) were made with a UV photometric TEI Model 49 analyzer (Thermo Electron Corporation, Franklin, MA, USA). The instrument was calibrated against a laboratory standard monitor (which was referenced against the NIST Ozone Standard Reference Photometer) prior to field deployment. Precision and accuracy were in the range of 1-2 ppbv and 0.5-1.5 ppbv, respectively. Measurement resolution was 1 minute, and the data was further averaged for posterior analysis.

3.6.2 Wind speed and direction

Wind speed and wind direction measurements (by INSTAAR) were made using a wind vane with a coupled three-cup anemometer (Model 034B-L, Campbell Scientific, Inc., Logan, UT, USA) at a height of ~ 4 m, at the Met Tower (see Figure A.1). Measurement resolution was 1 minute, and the data was further averaged for posterior analysis.

In summer 2009, the wind set broke and the wind speed measurements were replaced by the measurements of one of the three-cup anemometers (Model 010C, Met One Instruments, Grant Pass, OR, USA) located at ~ 2 m above the surface at the Met Tower (see Figure A.1). Measurement resolution was also 1 minute, and the data was further averaged for posterior analysis.

3.6.3 Radiation

Incoming and reflected solar radiation was measured using pyranometers (Model LI200X, Campbell Scientific Inc.) ~ 10 m west of the Met Tower on a pole, at ~ 1.4 m height above the surface. Measurement resolution was 1 minute, and the data was further averaged for posterior analysis.

3.6.4 Snowpack Temperature

Thermocouples type-E (Omega Engineering, Inc., Stamford, Connecticut, USA) covered by white shrink tubing to reduce radiation artifacts were attached at the middle of each of the cross bars of the Snow Tower to measure the snowpack temperature at each sampling level. Measurements were made with 1-min resolution and further averaged for posterior analysis.

4. RESULTS AND DISCUSSION

This chapter presents the measurements obtained during the 2 years of experiment. The chapter is divided in 2 sections. First, the seasonal behavior of nitrogen oxides within the snowpack is analyzed and the main features of the seasonal pattern are discussed considering changes in radiation, influence of wind and other factors. The following section compares the variability on diurnal cycles between spring and summer and discuss possible explanations to the behavior observed.

4.1 Seasonal characteristics

Figure 4.1 presents a contour plot of daily averages of NO_x mixing ratios over time and along the depth of the sampled snowpack. Short periods of instrument malfunctioning or sections where data was eliminated by the screening process were interpolated over time to help with the interpretation of the contour plot. During winter months, NO_x concentrations in the snowpack are in the range of 10-20 pptv, which is similar to the ambient concentrations measured during these months (~ 20 pptv). A clear increase in concentrations is observed during the spring and summer seasons, when sunlight reaches the snow. This increase is explained by the photochemical nature of the reactions producing nitrogen oxides within polar snowpacks. The magnitude of nitrogen oxides observed within the snowpack at Summit during the sunlight seasons measured here is on average 212 ± 119 pptv with maximum value of 530 pptv for 2009, and 102 ± 117 pptv with a maximum value of 557 pptv for the period measured in 2010. Previous measurements within the Summit snowpack at a depth of 10 cm were made by Honrath et al (1) during a particular day in summer. These measurements showed levels of NO_x in the interstitial air on the order of 300

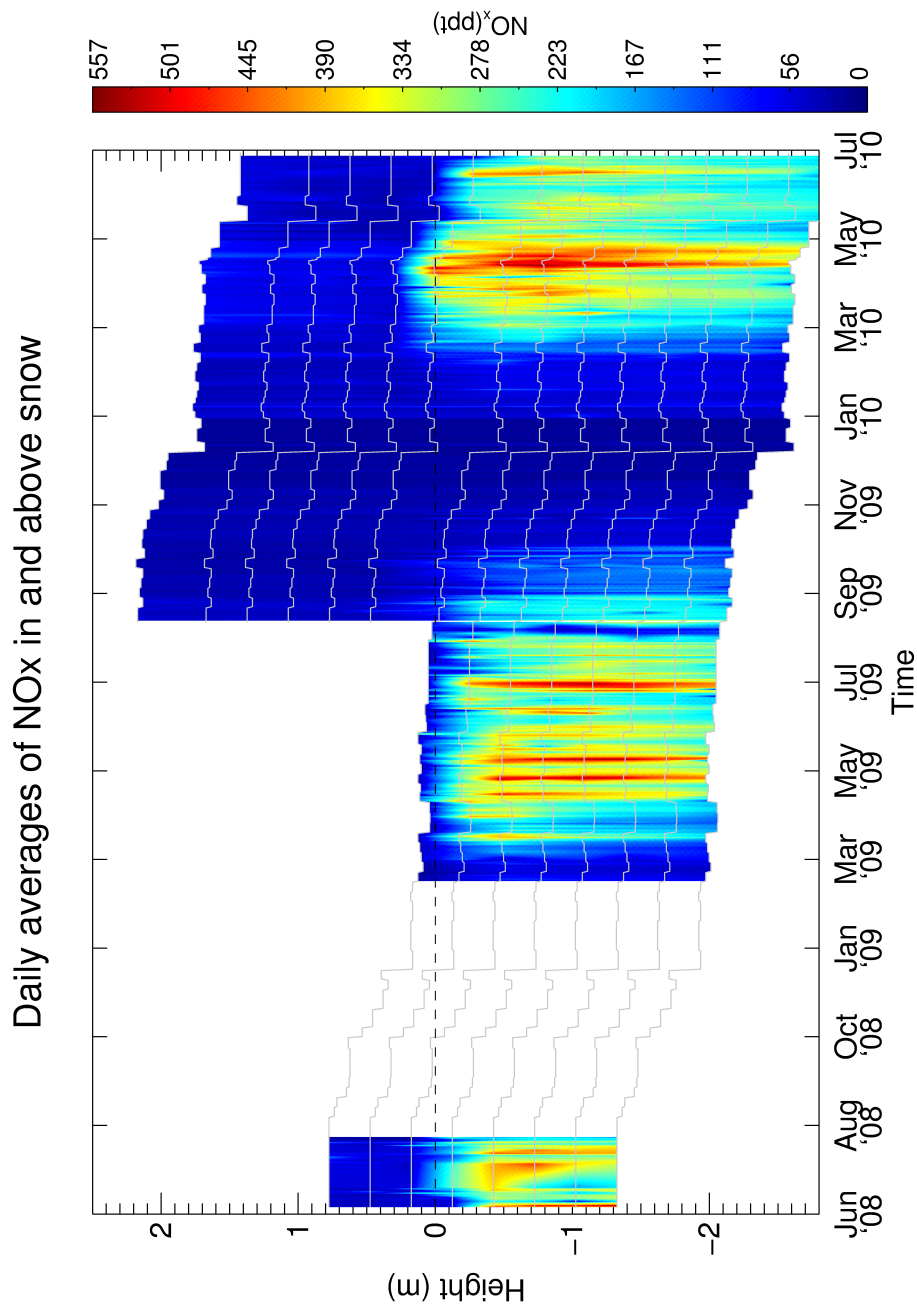


Figure 4.1. Daily averages of NO_x mixing ratios within and above the snowpack between June 2008 and July 2010. Gray lines represent the actual location of the sampling inlets. Black dashed line represents the surface of the snowpack. White sections are periods with no data.

pptv. Other than this experiment, there are no extensive campaigns of interstitial air sampling at Summit at the depths presented here nor year-round. To compare with experiments at midlatitudes, NO_x measurements within the alpine snowpack at Niwot Ridge, Colorado showed values of 10-15 ppbv (19). The values at Niwot Ridge represent mainly a biological source located in the soil underneath the snow. In contrast, the measurements at Summit could be considered as a 'background' reference for NO_x produced purely from photochemical reactions in a remote polar snowpack. This last consideration must be done having in mind that Summit presents rather unique conditions regarding long-range transport of pollution, as in many of the Arctic sites where this measurements could eventually be carried out. Anthropogenic sources can increase the amount of nitrate deposited onto the snow and its influence is larger in Arctic sites compared to Antarctic polar sites, where most of the nitrate sources come from marine air masses. Therefore, the values presented in this work could be considered as an upper limit of the amount of nitrogen oxides produced by snowpack photochemistry.

The contour plot presented in Figure 4.1 allows comparison of the 3 active seasons where snowpack measurements were taken. During summer of 2008, ambient NO_x mixing ratios (3 m above the surface) were 40-60 pptv. In contrast, the 3 upper levels of the snowtower located right above the snow surface show ~ 100 pptv of NO_x . This enhancement on NO_x mixing ratios detected at the levels close to the snow surface is most likely due to NO_x emissions from the snowpack. Unlike the upper levels of the snowtower, the levels within 50-60 cm of depth show mixing ratios on the order of 400-500 pptv which are the highest values detected that season within the snowpack. These values can also be detected for short periods at deeper levels, suggesting transport of gases from upper layers of the snow.

Unfortunately, after August of 2008 the instrument had to be switched off for almost all the winter of 2008-2009 due to malfunctioning and was not possible to fix it and keep it running continuously again until February 2009. Sampling started again in middle February, allowing it to capture the onset of photochemical activity within the snowpack. An increase in NO_x concentrations can be appreciated starting in middle March, although detailed time series of each sampling inlet allows to see that activity started as early as late February.

Similar patterns observed during summer of 2008 are also appreciated during 2009 season. The first level within the snowpack is located at an average of ~ 20 cm depth and it shows NO_x mixing ratios 2-3 times higher (~ 250 pptv) than the level right above the surface. The section of the snowpack below 50-60 cm shows the highest values, similar to what is observed in the previous summer. During April and May, there are 3 clear periods where it is possible to detect mixing ratios of the same order of magnitude observed at the photochemically active zone all the way down to the bottom inlet. Previous studies of the nitrate photolysis rate coefficients at Summit revealed that $J_{\text{NO}_3^-}$ decreases logarithmically with depth and at 50 cm within the snowpack is close to one order of magnitude less than at the surface (83). In addition, modeling studies indicate that just 1-4% of the surface actinic flux ($\lambda < 350$ nm) can penetrate to 50 cm (84). Thus, the detection of high mixing ratios at levels deeper than the characteristic e -folding depth of the light must be due to ventilation effects of the upper levels of the snowpack and will be discussed with greater detail in section 4.1.1.

An apparent increase in NO_x can be observed at the end of August 2009 at all levels within the snow. This apparent increase is most likely the effect of digging around the snowtower which was done to install the new extension that allowed to measure above the snow. The installation was done right at the end of the summer season, to give enough time to the snowpack to adjust naturally over the winter. During 2010, similar characteristics are observed. Increase in NO_x within the snow is appreciable since late February-early March and high values are focused between 50-60 cm. During spring months, an increase in concentrations can be appreciated within the first 30 cm above the snow, which could correspond to NO_x emissions from the snowpack.

Maximum total NO_x measured within the snowpack column during each year, 2009 and 2010, is ~ 550 pptv. This suggests that the photolytic production of NO_x is similar during both years independently of other factors that could affect the photolytic processes responsible for NO_x production, for example, nitrate availability. This observation could also imply that either the sources of nitrate remain somehow constant and thus Summit was exposed to a similar amount of anthropogenic and natural sources during both years, or that no matter how much nitrate is present in

the snowpack, the degree of nitrate photolysis remains constant at the atmospheric and meteorological conditions of Summit. Nonetheless, to verify any possible trend in NO_x production within the snowpack, it is necessary to have long-term measurements since two years are not enough to determine interannual variability. A separated contour plot of each year is presented in Figure 4.2. It is also interesting to observe that marked enhancements within the snowpack are detected at similar periods of the season.

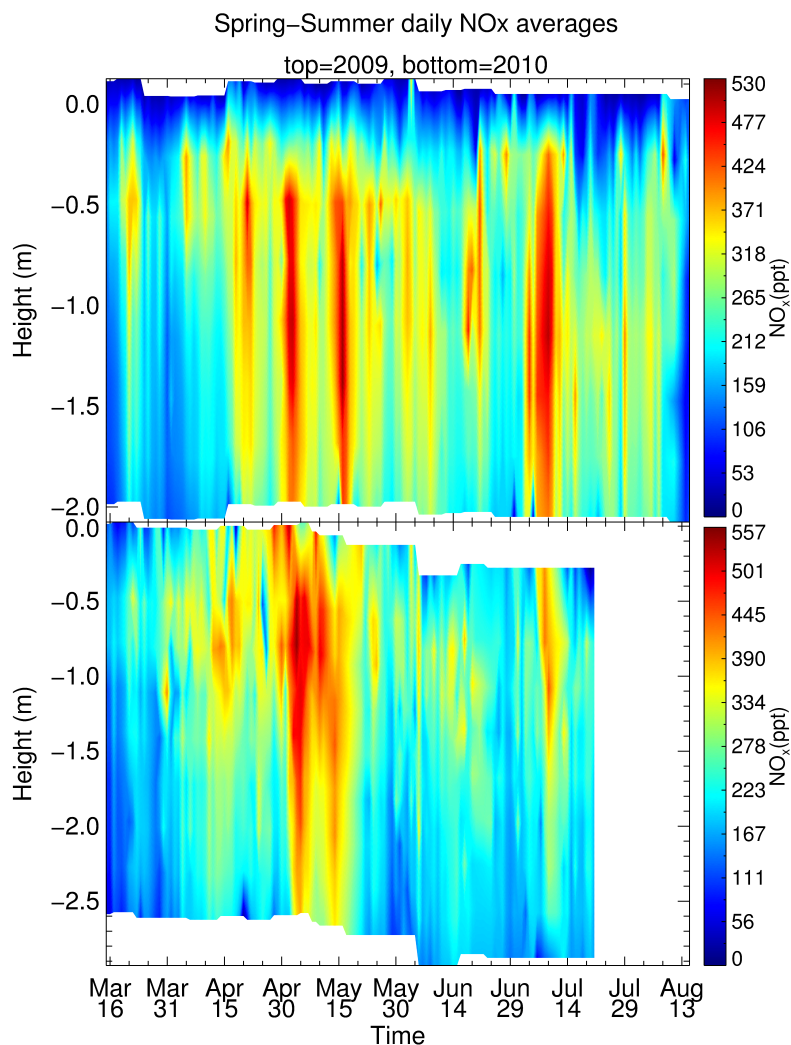


Figure 4.2. Contour plot of NO_x mixing ratios within the snowpack for each year.

4.1.1 Wind influence on NO_x distribution within the snow

Wind and surface roughness act together to induce pressure variations which in turn drives ventilation and/or interstitial air flow through the snow. Albert and Hawley (85) studied ventilation properties at Summit and revealed that depending on the size of the surface roughness, high wind conditions ($>12 \text{ m s}^{-1}$) can induce airflow between 2 and 4 m into the snowpack. Figure 4.3 shows mixing ratios within the snow and wind speed during the spring-summer season of 2009. In this figure it is possible to observe that during the periods when high NO_x values are detected at ~ 2 m within the firn usually events of moderate to high wind speed can be also observed. A comparison with ozone values within the snowpack showed the same behavior for this specie.

Looking closer to the time series presented in Figure 4.3, NO_x mixing ratios at 80-150 cm depth show particularly a delay of ~ 24 hrs in their maximum respect to the peak in wind speed. A possible explanation for this delay is the variation in permeability through the snowpack. Albert (86) established the importance of considering firn layering. The study shows that snowpack permeability at Summit varies at least a factor of 10 over the top 3 m, with a surface layer of approximately 50 cm of lower permeability than the underlying firn. The effect of a lower-permeability surface layer is to decrease the air flow in the underlying firn, which would cause the delay between the peak on wind speed and the detection of higher mixing ratios at deeper levels. It must be mentioned that ventilation velocities reported (85) for winter under high winds are in the order of 3 cm s^{-1} and 1 cm s^{-1} for summer, both values considerably higher than what would be expected to explain a delay of the magnitude observed. Although these reported values are the product of a modeling study that could be overestimating the actual velocities, it must be considered the possibility of other variables increasing the time of transport to the underlying firn, such as NO_2 interactions with the aqueous surface of the snow grains. Although studies discarded the relevance of NO_x adsorption on ice (87), others have found that NO_2 hydrolysis on surface is indeed efficient (93) and it also has been speculated that reactions of NO_2 on irradiated ice surfaces containing humic acid substances to form HONO is accelerated in the presence of visible light (88). Nonetheless, the time scale of these processes cannot explain the delay observed.

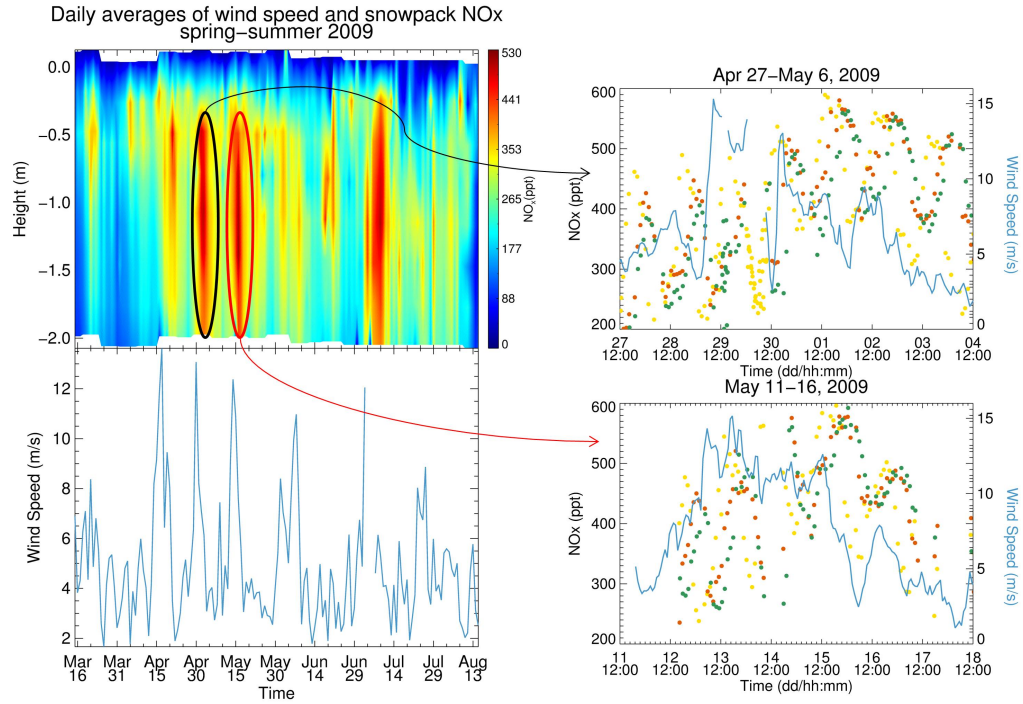


Figure 4.3. Contour plot of daily averages of NO_x in the snowpack (left, top) and daily averages of wind speed at 7 m above surface (left, bottom) for spring-summer 2009. Detailed time series of NO_x (4 h average) and wind speed (1 hr average) are shown (right) for each specific event circled in the contour plot at left. NO_x mixing ratios showed at right correspond to 80 (yellow), 110 (orange) and 140 (green) cm depth.

In addition, under sustained pressure forcing conditions it is possible to have higher velocity air flow in the more permeable deeper layers, as a result of increased horizontal flux and net air flow within the layer (85). Steady-state surface pressure forcing conditions are likely to occur when winds are sustained, which is typically observed at Summit and other polar sites where once windy conditions develop, they can last for days. This is the situation observed in Figure 4.3 where moderate to high wind speed conditions are observed for a period of 4-5 days. The increase in air flow in the more permeable layers would explain the almost negligible difference in mixing ratios between each of the levels shown in Figure 4.3.

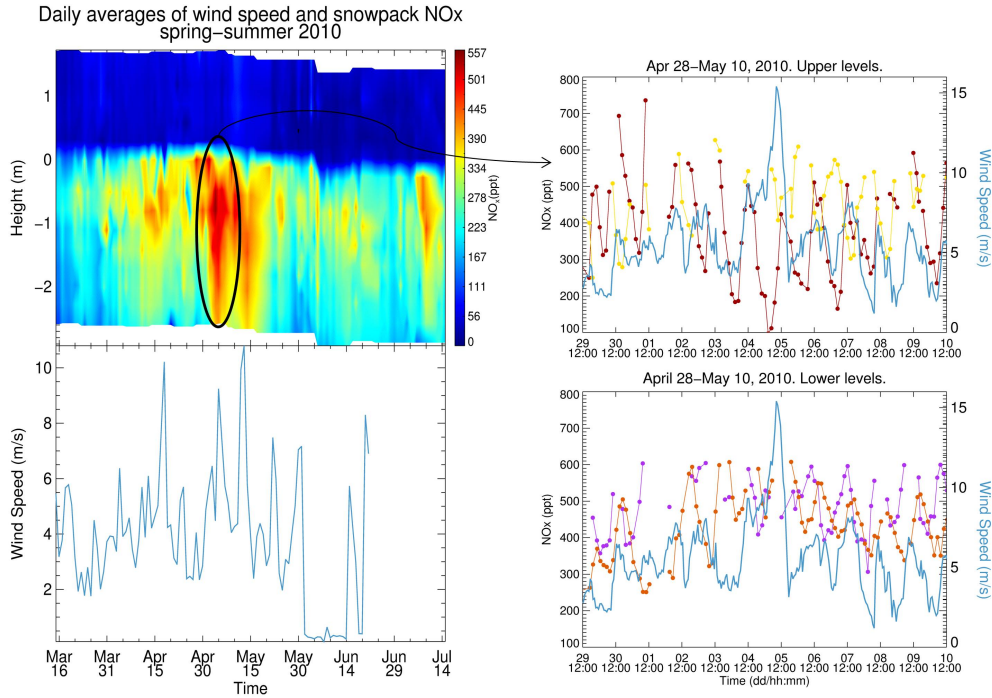


Figure 4.4. Contour plot of daily averages of NO_x in the snowpack (left, top) and daily averages of available wind speed data at 7 m above surface (left, bottom) for spring-summer 2010. Detailed time series of NO_x (4 h average) and wind speed (1 hr average) are shown (right) for the event circled in the contour plot at left. NO_x mixing ratios showed at top right correspond to ~0 (dark red) and 50 (yellow) cm depth; bottom left shows NO_x mixing ratios at 80 (purple) and 110 (orange) cm depth.

Spring of 2010 was extremely difficult to keep the instrument running constantly due to continuous issues with the generator of the camp site. Numerous random power outages affected the measurements causing gaps in the data. In addition, during spring 2010 there were more periods with N winds compared to what was observed during 2009. Thus, the dataset corresponding to this season contains a larger amount of interpolated periods. The main enhancement event observed in 2010 that contains actual data without interruptions shows a different behavior compared to what was observed during this same type of periods in 2009. A figure similar to what was shown for 2009, is presented in Figure 4.4 for 2010.

In this case, the wind effect cannot be assigned as responsible for an increase in NO_x mixing ratios at lower levels. A rise in NO_x at the level closest to the surface is observed in April 30 (Figure 4.4, top right, dark red), before the major event in wind speed and it seems to be causing the raise observed at levels below. The increase at surface level must be response to a chemical factor that is not possible to determine with the current measurements. The only relevant factor that could make a difference is that according to the field logbook, the night of April 28 was extremely foggy. Previous studies have shown that fog episodes tend to increase deposition of HNO_3 (8) onto the snow. If NO_3^- is included in the QLL, it could constitute an extra source of NO_x in the surface layer that would explain the increase observed in NO_x , but also it would be expected to observe an increase the next day (April 29) instead of the day after (April 30). Since this is not observed, it is not possible to determine a reason for the increase observed in the surface levels. May 5 is the day where winds peak, and no change in concentrations at lower levels is observed after this event. The only response detected is at the surface level where concentrations decrease drastically as effect of windpumping. The reason of why is not possible to observe the same effect detected in the previous year is not known.

Summarizing, presence of high mixing ratios in deep layers is, if not the effect of inflow from upper layers during high wind speed events, the result of molecular diffusion along the snowpack. From the contour plots in Figure 4.1 is easy to see that an important amount of NO_x is present in layers underneath during the complete season, even under low wind conditions. This constant presence is explained by vertical transport through molecular diffusion, driven by concentration gradients between layers where sunlight penetrates and deeper layers where no photolytic process can occur. Movement of a gas in the snow under pure molecular diffusion conditions, in the absence of ventilation, is roughly 0.03 cm s^{-1} (85). Summit boundary layer dynamic is influenced by diurnal, summertime radiation cycles that contributes to the growth and mixing of the boundary layer and provides regular ventilation conditions (89). Therefore, it would be expected that a constant transport of gases from the upper layers to the layers underneath is occurring, and most of the time this molecular movement is increased by the regular ventilation conditions of Summit, with particular high wind speed events producing maximum vertical transport.

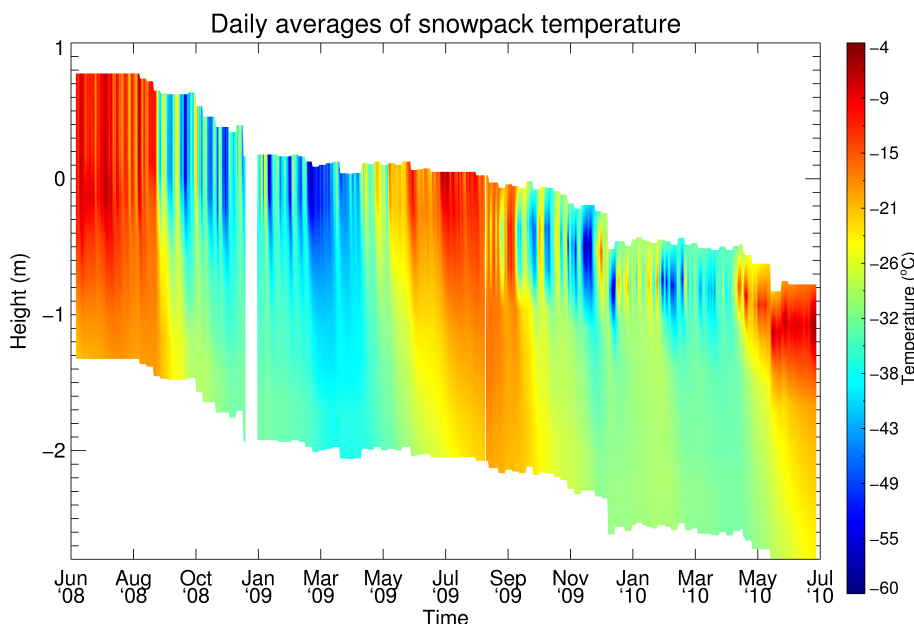


Figure 4.5. Diurnal averages of snowpack temperature.(Preliminary data courtesy of Brie Van Dam,INSTAAR.)

4.1.2 Influence of snowpack temperature

Previous studies with snow-piles in Alert (5) have mentioned the possibility that light alone cannot explain the production of significant amounts of NO_x and hypothesized that there should be a temperature threshold that is function of the snow crystal type, that induces NO_3^- diffusion to the surface of the snow crystals facilitating photolysis process that produces gas phase NO_2 . Figure 4.5 shows a contour plot of diurnal averages of snowpack temperature through the experiment.

An increase in temperature of approximately 15°C is observed at the beginning of May during both years. During the beginning of the sunlight season and the onset of photochemical activity during 2009, the temperature of the snowpack is approximately -50°C and during 2010 approximately -40°C . These results show that there is no change in temperature within the snowpack during the onset of photochemical activity detected at Summit, nor during the maximum production observed for NO_2 during early spring. This could imply that NO_3^- ions are easily available at the surface of the snow grains and then the NO_2 produced diffuse to the firn air independently of the cold temperatures detected within the firn. The warmest period measured is from

May to late August and the increase in temperature actually matches the decrease in NO_2 production. This apparent match is more likely to be an effect of the increase in radiation rather than an effect of the temperature. $\text{N}_{(III)}$ species has a much larger light absorption in the UV-A than NO_3^- , where actinic fluxes are relatively larger compared to the UV-B. Thus, the NO_2^- formed would be immediately converted to NO (51,52) instead of being converted to NO_2 . The warm period correlates with the highest levels of NO measured but does not coincide with the first NO enhancements observed during March. Finally, from the measurements is possible to confirm that there is no change in snowpack temperature that could influence the beginning of photochemical activity.

4.1.3 NO and NO_2 profiles.

Individual plots of NO and NO_2 allow appreciation of differences in the distribution of each species within the snowpack and also to determine the main component of NO_x . Figure 4.6 shows a contour plot of each specie during 2009 and 2010. It is obvious from these plots that NO_2 is the main component of NO_x within the snowpack at Summit. The larger presence of NO_2 respect to NO ($\sim 90\%$) could be explained by the fact that this specie is the main product of nitrate photolysis. As it was discussed previously in section 2.4.2, nitrate photolysis can follow two pathways and reaction 2.1 (which produces NO_2) exceeds the second channel roughly for a factor of 8 or 9. In addition, NO_2 can only be photolyzed in the upper layers of the snowpack and the remaining will be transported to levels underneath, where no photolytic losses or advection by wind can affect it. Another possible explanation that must be mentioned is that most of the NO that could be formed as product of NO_2 photolysis, reacts with O_3 to form NO_2 causing high concentrations of NO_2 with respect to NO. O_3 concentrations within the upper levels of the snowpack are in the order 40 ppbv during the spring and early summer and decrease to about 20-30 ppbv at the end of the sunlight season (see Figure 4.7). Nevertheless, the excess of O_3 within the snowpack relative to NO_x is enough to consume all the NO present at all times of the season, therefore the detection of increasing NO concentrations at some point during April-May suggests that O_3 is not destroying all the NO produced.

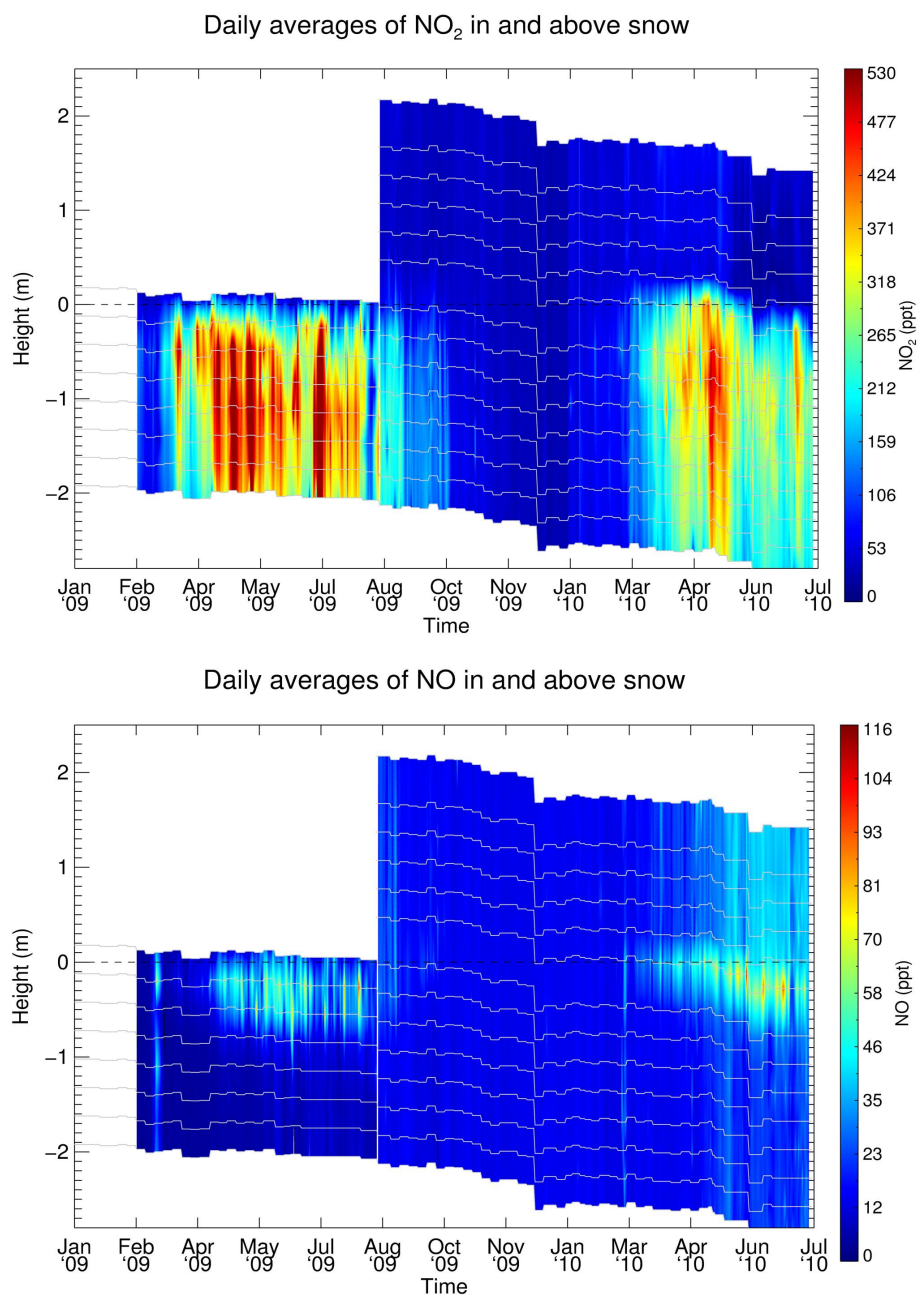


Figure 4.6. Daily averages of NO₂ and NO for year 2009 and 2010. Black dashed line represents the surface of the snowpack.

Besides the larger difference in mixing ratios between each species, a different distribution within the snowpack is also observed. NO is mainly present in the upper levels (~ 50 cm) of the firn, while NO₂ can be detected mostly in the layers underneath with some overlap between NO and NO₂ between 20 and 50 cm depth. The presence of NO mostly in the upper layers is explained by the fact that this molecule is the direct product of NO₂ photolysis. It could also respond to the photolysis of nitrite under acidic conditions (reaction 2.6 reverse) which produces NO and hydroxyl radicals. Organic compounds present in snow can consume OH and therefore allow NO to persist within the upper layers. Since it is mainly located in the area closer to surface, the continuous advective ventilation caused by wind will release most of the NO produced to the overlying atmosphere. An increase in ambient NO concentrations detected at the levels above the snow can be observed after April 2010, which could be attributed to snow emissions. The study of ambient gradients and fluxes can give further information on this topic but it is beyond the scope of this thesis and will be matter of future work.

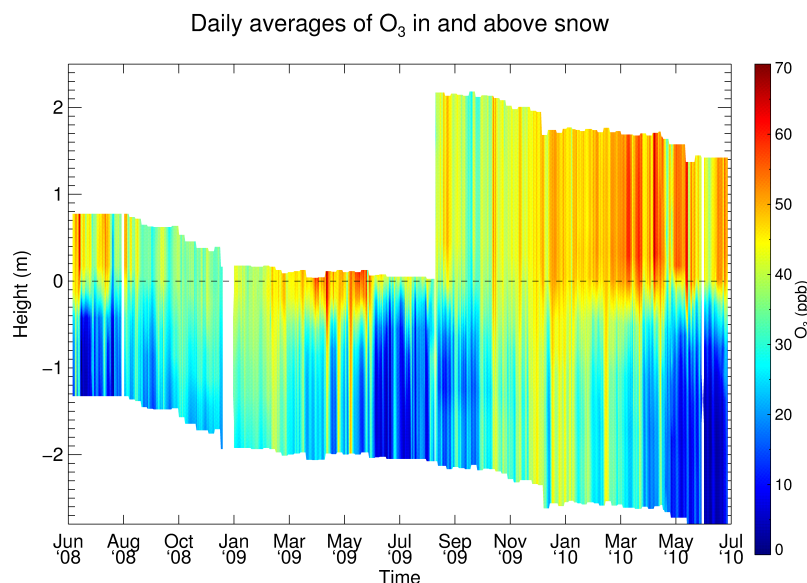


Figure 4.7. Daily average of O₃ mixing ratios within and above the snowpack between June 2008 and July 2010. Black dashed line represents the surface of the snowpack. (Preliminary data courtesy of Brie Van Dam, INSTAAR).

An interesting analysis of the photochemical behavior of these species can be done by plotting the snowpack data and incoming radiation over the sunlight season, as showed in Figure 4.8. The maximum of NO_2 mixing ratios is observed in early spring, before the maximum in incoming radiation. On the other hand, NO follows exactly the increase and decrease in radiation over the season. This can be explained by the differences in absorption properties of each source. NO_3^- is a UV-B absorber and thus the production of NO_2 is going to be influenced by the same factors that affect UV-B radiation availability: O_3 total column and solar zenith angle. NO_2 , on the other hand, is a UV-A absorber and NO production will depend mainly on factors like clouds, aerosols, albedo, etc. (see section 2.2).

Considering these differences, possible reasons that explain the shift in the maximum for NO_2 respect to radiation could be: first, a direct relationship with the stratospheric O_3 decrease in spring. Although stratospheric ozone depletion in the Arctic is not as marked as in Antarctic (90), records in many stations show a degree of O_3 depletion during March that could cause an increase in the amount of UV-B that reaches the surface and thus an increase in the radiation wavelengths that favor the photolysis of nitrate during early spring. For Summit, this decrease is not particularly relevant; the ozone column data recollected by the National Oceanic and Atmospheric Administration (NOAA) shows a stable value around ~ 400 DU (91) for spring during years were snowpack measurements were taken, thus this option can be discarded.

A second option is that NO_2 maximum during spring could be the result of not enough radiation to cause a relevant degree of NO_2 photolysis. Since NO follows total incoming radiation, is then reasonable to assume that the degree of NO_2 photolysis is not relevant until certain level of radiation is available. To determine if seasonal variations in the spectral properties of incoming radiation are related to different levels of production of these species, measurements of spectral irradiance would be required and thus, is not possible to verify this hypothesis with the current measurements. A third option would be an increase in sources of NO_2 during spring but studies of NO_3^- concentrations in Summit have shown that there is no clear seasonality in concentrations of NO_3^- in surface snow (92). Therefore, with the current measurements it is difficult to determine a specific cause for the offset in NO_2 mixing ratios.

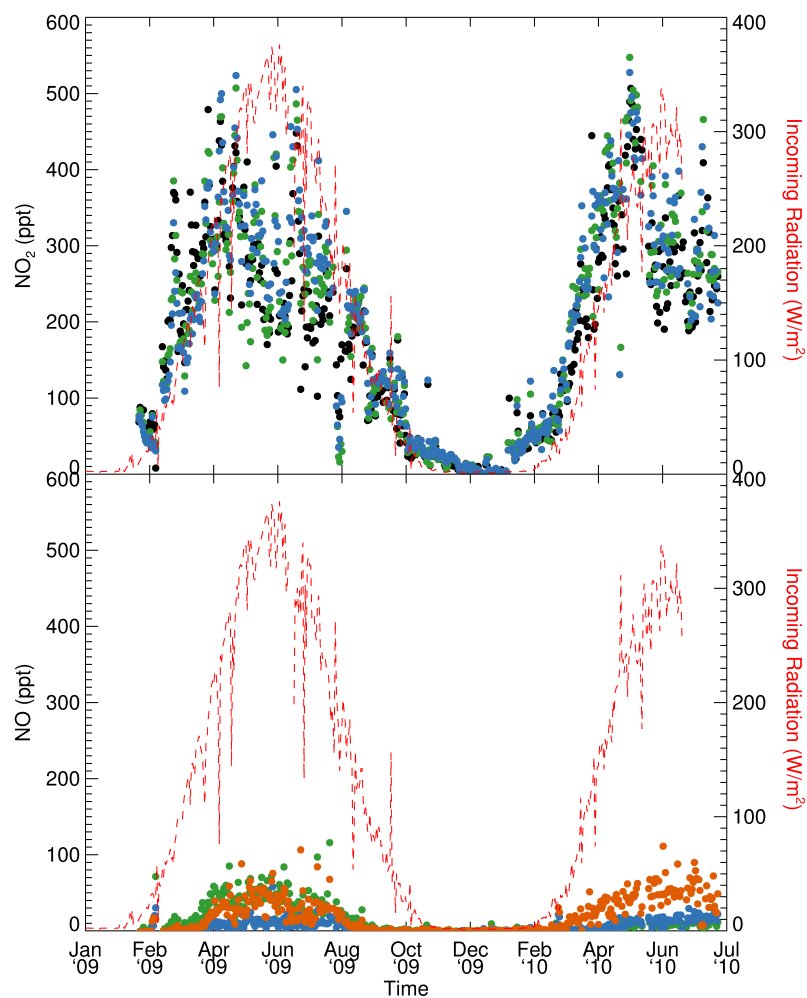


Figure 4.8. Daily averages of NO_2 (top) and NO (bottom) enhancements (respect to ambient concentrations) within the snow for 2009 and 2010 seasons at levels of photochemical activity. Daily averages of incoming radiation are shown in red. Levels shown represent roughly the same section of the snowpack for both years (~ 1 m depth). (Preliminary radiation data courtesy of Brie Van Dam, INSTAAR.)

4.2 Diurnal Cycles

Since nitrogen oxides are product of photochemical reactions, is expected to observe diurnal cycles with a different degree of development depending on radiation and other conditions. The analysis of diurnal cycles for NO_x over the season gives primary information about when the photochemical production reaches a maximum, the relationship with the amount of radiation available, and the differences in magnitude for NO and NO₂ over the photochemically active season. It also can provide information on how the variables mentioned above have different patterns at different depths within the snowpack, and then it allows to setup basic ideas to understand the behavior observed for each species.

Figure 4.9 shows diurnal cycles for the three levels close to the surface. Each box represents an average of 2 hours of NO_x enhancements within the snow, and each time of the day has been monthly averaged to produce a diurnal cycle representative of each month. Enhancements (ambient data subtracted) were chosen to highlight when the production of NO_x within the snow becomes relevant over the ambient mixing ratios. The left axis represents the NO_x enhancements expressed in pptv and incoming radiation has been plotted as reference on the right axis. There is no radiation data for June 2009 due to a malfunction of the radiation sensor. From left to right each plot represents one month, from February to August of 2009. From top to bottom, each row represents a different level within the snow, with the top row being the level closer to surface. The top three levels located within the snowpack during 2009 were chosen to describe the photochemical behavior of NO_x because they are located within the photochemically active zone.

Data presented corresponds to 2009 since it is the year with a set of measurements for the complete sunlight season. Statistically speaking, the dataset for NO_x enhancements during 2009 is not evenly distributed. Though the mean and median are usually close to each other, they are not usually located at the middle of the data. This indicates that the data is usually clustered either at low or at high values. There is a greater amount of outliers observed on the upper extreme of the data.

The onset of photochemistry within the snowpack is observed in February, with the smallest amounts observed for each level, on the order of 20-30 pptv at 20 cm

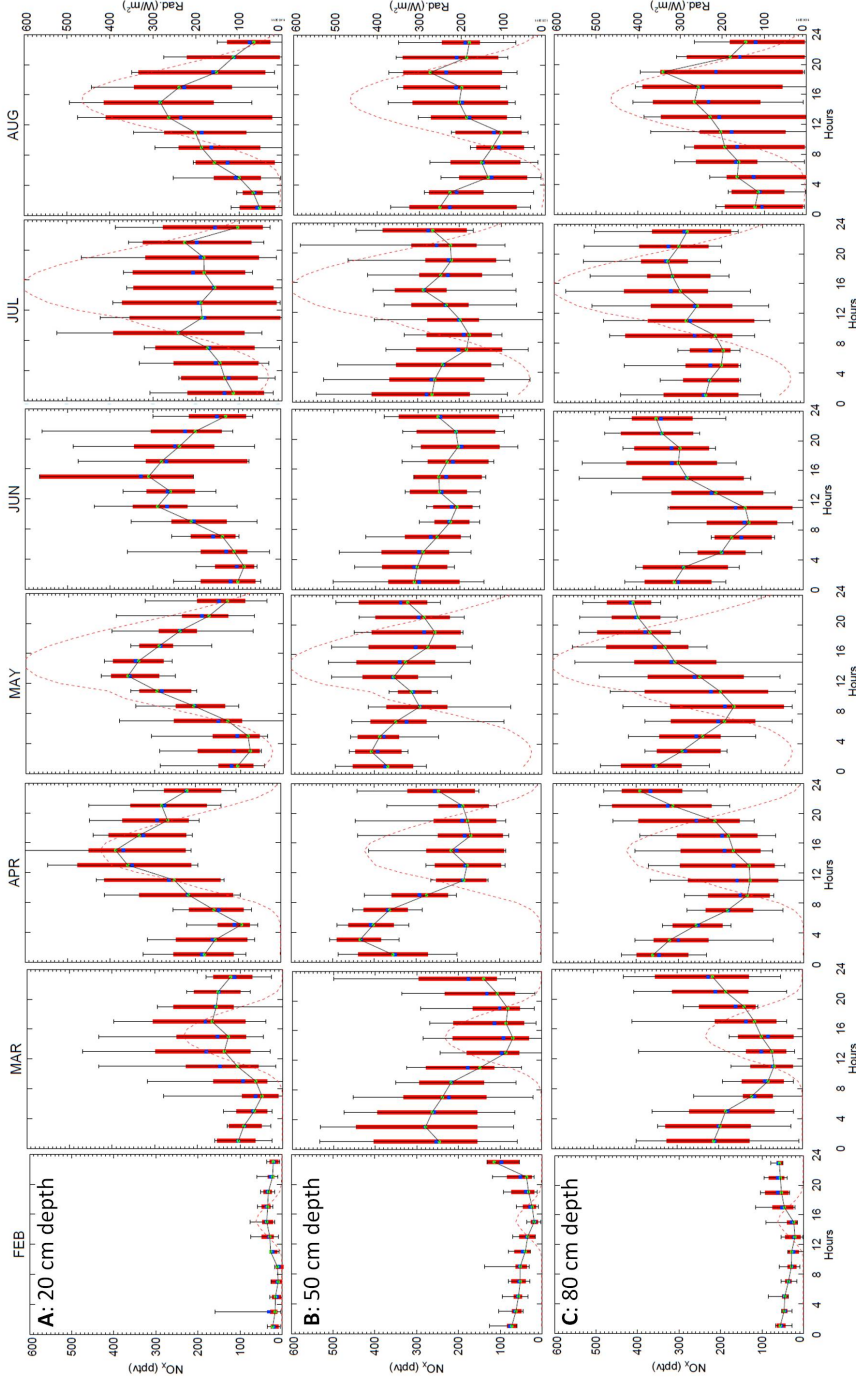


Figure 4.9. Box plots of NO_x enhancements within the snow for three different depths, showing the average diurnal cycle for each month during spring-summer 2009. Each box represents an average of 2 hours of data. Black line represents the range between 5-95 quartiles, red box represents the range between 33-67 quartiles, green dot is the median and blue box is the mean for each set of data. Radiation data is plotted as a thin red line. Left axis represent NO_x mixing ratios and right axis represent radiation data. Time is presented as UTC, therefore local noon corresponds approximately to 3 pm.

depth and 50-80 pptv at deeper levels, somewhat higher than at the level closer to surface. Slightly larger values (roughly 50-100 pptv) are observed most of the time at deeper levels. An increase of almost 100 pptv is observed for all levels showed between February and March, which is related to an increase of $\sim 200 \text{ W/m}^2$ in incoming radiation.

Level A shows a peak on mixing ratios coincident with the maximum in radiation for almost all the season, except by July where the peak on the diurnal cycle is lost. After this break in the pattern, a rather steep diurnal cycle is observed again in August, where the mixing ratios during night and early morning are somewhat smaller than the observed values during previous months. Level B shows a minimum coincident with the maximum in radiation during March. During April and subsequent months, the minimum observed is suppressed by a small increase in NO_x production, that shows its maximum at times of maximum insolation. The maximum concentrations are still observed during nighttime, but this small increase in NO_x production seems to compensate the destruction observed at daytime, particularly during May, June and July. During July, level B shows mixing ratios increasing again at late evening and keep their levels overnight. Finally in August, an increase is observed at late evening that reaches similar magnitude to levels measured at midnight.

At level C the minimum is observed earlier than for level B, during morning. The magnitude of concentrations increases over the season, ranging from maximums of ~ 200 pptv in March to ~ 400 pptv in April, and later in the season decreasing to ~ 300 pptv. Despite these variations, the minimum at early morning is observed markedly and consistently during spring and early summer. In July the minimum is compensated by a small increase during morning, concentrations do not vary as much over the day and the maximum is observed during early afternoon. At the end of summer, level C shows a clear diurnal cycle with a maximum observed at late afternoon.

New information about the photochemical processes governing the diurnal cycle observed for NO_x can be obtained by analyzing the diurnal cycles of each specie at levels with photochemical activity. Figure 4.10 shows the same box plots used to describe NO_x diurnal cycles, but now they are showing NO and NO_2 independently for levels located at 20 and 50 cm depth.

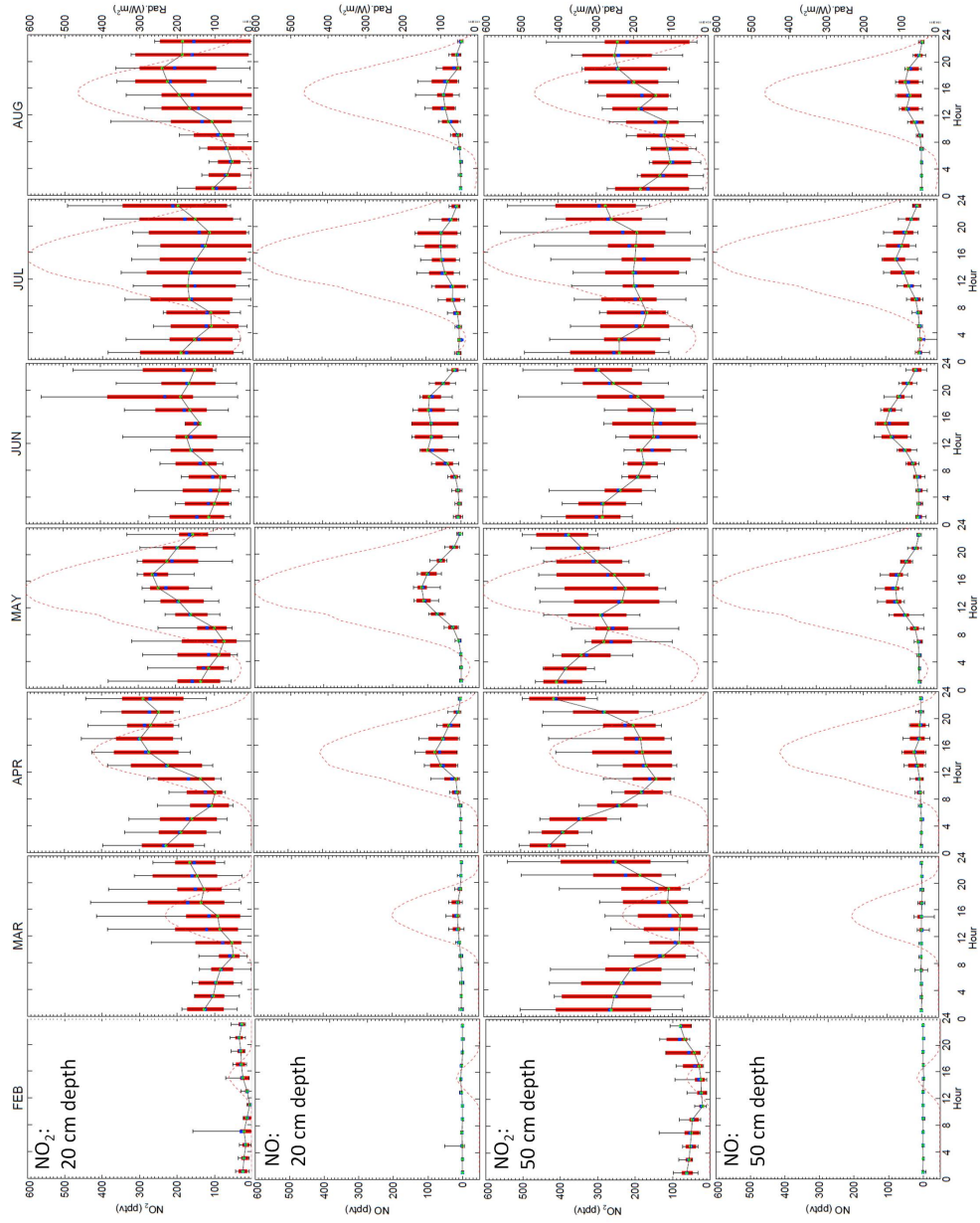


Figure 4.10. Box plots of NO₂ (first and third rows) and NO (second and fourth rows) enhancements within the snow for the first 2 levels showed in Figure 4.9. The description is similar to box plots showed before. Time is presented as UTC, therefore local noon corresponds approximately to 3 pm.

The low concentrations observed during February, when photochemistry is slowly becoming relevant, correspond entirely to NO_2 enhancements. Close to the surface a slight decrease in NO_2 at early morning is observed, as well as in the level underneath. This decrease in NO_2 is not reflected in an increase in NO , which could just mean that the degree of NO formed by NO_2 photolysis does not overcome the observed ambient concentrations, and thus the enhancements within the snow remain negligible. Another possible reason could be that the small amounts of NO present within the snow rapidly react with O_3 and form NO_2 . In Figure 4.7 is possible to see that O_3 within the snowpack is higher during spring than during summer of 2009, and it could suggest that a decrease in O_3 within the snowpack caused an increase in NO mixing ratios during summer, but the large difference in magnitude between mixing ratios of NO (pptv) and O_3 (ppbv) makes difficult to attribute to NO any change in O_3 concentrations. Vice-versa, the existence of 100 pptv of NO in average over summer while O_3 is close to 3 orders of magnitude larger gives the idea that O_3 is not the main sink for NO in the firn.

During March and April, NO_2 mixing ratios at 20 cm depth show a diurnal cycle with a maximum slightly off from the radiation peak, and a minimum during early morning. April is the month where the highest mixing ratios for NO_2 are detected, with enhancements of ~ 300 pptv slightly after noon. During May, it is a similar pattern, except that NO_2 mixing ratios decrease during late evening hours. In June the diurnal cycle is very weak, and during July the variability in mixing ratios is very small, with two weak minimum points at early morning and local noon. Finally, in August the diurnal cycle is restored again with values ranging between 50-200 pptv and a maximum observed at evening hours.

NO at 20 cm depth shows the smallest enhancements in March, and during all the season ranges between 0-100 pptv with the maximum measured corresponding to May. Each monthly profile correlates perfectly with radiation which suggest that NO is exclusively a photochemical product, most likely from photolysis of NO_2 within the gas phase. Assuming no gas-phase chemistry, other alternatives for NO formation could correspond to photolysis from HONO within the QLL. Nitrous acid could be formed from hydrolysis of NO_2 through reaction 4.1:



Besides the possibility of hydrolysis within the QLL, reaction 4.1 has also been found to occur easily on ice surfaces (93) and also being enhanced on surfaces doped with humic like substances (see 2.4.3). Although the low levels of NO could be explained by photolysis of NO₂ in the gas-phase that is much slower than reactions in the aqueous phase, it is not possible to rule out as NO source the photolysis of HONO coming from heterogeneous reactions or processes within the QLL.

At 50 cm depth, NO₂ profiles show higher values, a clear minimum during morning hours and maximum over night. The increase of mixing ratios overnight could correspond to continuous transport from the upper levels after the photochemical production has stopped in layers above. NO₂ values range from 100-300 pptv during March to 200-400 pptv in May. Later in June, the magnitude of NO₂ decreases and the minimum in the diurnal cycle is observed at noon. In July, it seems possible to detect a degree of compensation at noon time showing a rather flat profile at times where a minimum is observed during the previous month. August shows a diurnal cycle again with smaller enhancements, and a maximum at late evening. NO at this level shows the same behavior observed in upper layers, correlating with radiation and maximum enhancements observed during months of high radiation. Interesting is to see that NO enhancements are detectable a month later respect to the upper layers, which could mean that NO transported from layers above is observed at 50 cm only when the production at upper levels reaches certain magnitude. The delay in the increase of NO at 50 cm could also be just the result of not enough radiation penetrating the snowpack during the first months of sunlight. Thus, just when radiation reaches certain levels, sunlight can penetrate deeper in the firn and cause photolysis of NO₂. This explanation is more representative of the observations, since even though there is a delay of a month, the daily profile does not show a delay and peaks of NO correlate with peaks in radiation at both levels.

In summary, the analysis of diurnal cycles help to improve the understanding of the distribution of NO_x within the snowpack. Production of NO₂ is observed at the level closer to surface which is located at 20 cm depth for most of the sunlight season during 2009. This depth is also within the range of reported *e*-folding values for

most of the snowpacks (29). This is confirmed by the fact that NO_2 diurnal cycles correlating with radiation levels are observed only at 20 cm depth and not in the level underneath. Although NO_2 levels correlate with radiation over the day, they do not correlate with radiation over the season. Maximum NO_2 levels are observed in April, while May-July are the months with highest insolation levels. This was also observed in Figure 4.8. NO measurements showed that this species is highly correlated with radiation at a diurnal and seasonal scale. Thus, the decrease of NO_2 at upper layers during months of high insolation could respond to a larger NO production from NO_2 photolysis. The presence of high levels of NO_x at 50 cm and below seems to respond exclusively to transport from upper layers. Although enhancements at this level are the highest measured within the snowpack, it is most likely due to a less degree of advection that allows gases to accumulate at deeper layers. NO profiles at 50 cm also support the idea that its presence at that depth responds to some degree of transport from layers above that becomes relevant once the production of NO at the upper layers increases. The reason of why the diurnal cycle for NO_2 during July is negligible at both levels analyzed (20 and 50 cm depth) is not clear. It is interesting that after this break in the observed pattern, a clear diurnal cycle is observed in August with maximum values displaced to late evening. Thus, July could correspond to a transition between chemical processes, that in the case of NO_2 at 50 cm depth, changes the profile from minimum detected during late afternoon to a minimum observed in early morning.

5. CONCLUSIONS AND FUTURE WORK

The purpose of this study was to characterize the NO_x budget within the snowpack at Summit, Greenland. This work was motivated by the need to improve the understanding of snow photochemistry at remote polar regions, an objective that was established as the first step of a larger research project that aims to parameterize air-snow interactions at a global level. The experiment was carried out at the Geo-Summit research station located at 3200 m above sea level, on the top of the ice cap in Greenland. Measurements were taken continuously from June 2008 to July 2010 to capture the seasonal variability of the production of nitrogen oxides within the snow, with a novel system that allowed to sample firn air with minimal disruption of the natural snowpack. In addition, measurements of meteorological variables and ozone within and above the snowpack were taken to investigate the possible influence of these parameters in the NO_x budget at Summit. The dataset obtained constitute the largest record of trace gases within the firn air of polar snowpacks, with measurements taken for the first time during winter and at depths greater than 1 meter. The results obtained in the analyses of these measurements are summarized in the following section. Based on the results obtained in this study, future work is recommended in order to improve the understanding NO_x exchange between the snowpack and the overlying atmosphere at Summit, Greenland.

5.1 Conclusions

This work focused exclusively on the analysis of measurements of NO_x within the snowpack at Summit. The seasonal variability was investigated through diurnal averages of the measurements. The influence of wind on the distribution of trace gases within the firn was studied by comparison of mixing ratios and wind speed time series. Possible influence of temperature on photochemical production of NO_x was investigated by comparing annual profiles of NO_x within the snow and snowpack temperature measurements. Profiles of NO and NO_2 were analyzed against incoming radiation profiles and ozone concentrations within the snowpack. Diurnal cycles were studied by monthly averages of measurements at different depths. The main conclusions are:

- **Nitrogen oxides concentrations within the snowpack increase during the sunlight season.** An increase in measured concentrations within the snow is observed during late February and continues during spring and summer while sunlight can penetrate the snowpack. This observation is consistent with previous studies that pointed towards a photochemical source within the snowpack, most likely NO_3^- photolysis within the QLL, as the source for NO_x within the snow (1, 49).
- **Nitrogen oxides production within the snowpack remained similar during both years.** The maximum values measured within the snow during each year were on the order of ~ 550 pptv despite observed differences between years in the magnitude of incoming radiation and possible differences in the amount of nitrate available for photolysis. This result suggest most likely that the variability of NO_x sources between both seasons was small and/or that the degree of photolysis of NO_3^- remains fairly constant independently of changes in incoming radiation.
- **High wind speed events induce inflow of NO_x produced in upper layers into deeper layers of the snowpack.** The presence of marked enhancements in NO_x mixing ratios at deep levels where photochemical processes

are absent correlates with events of high wind speed. This behavior was also observed in ozone mixing ratios within the snowpack. In addition, under low wind conditions vertical transport is induced and overcomes molecular diffusion, resulting in a constant transport of NO_x produced in upper layers to deeper layers. This suggest that ventilation conditions play an essential role in the distribution of trace gases within the snowpack and must be considered in modeling studies that attempt to parameterize air-snow interactions.

- **Snowpack temperature does not influence the onset of photochemical NO_x production.** During the period where the first NO_2 enhancements are detected, snowpack temperature is on the order of -40°C and there is no change that could be associated with the onset in nitrate photolysis. On the other hand, there is an increase in temperature at the beginning of May which coincides with the decrease in NO_2 concentrations and maximum NO concentrations detected. This suggest that nitrate availability for photolytic processes generating NO_x is not affected by the cold temperatures as suggested by previous studies (5) and is located very close to the surface of snow grains, allowing NO_2 easily diffuse to the firn air.
- **No evidence of strong relationship between NO_x and O_3 .** The comparison of profiles for both species shows that even though O_3 concentrations decrease during months with high NO mixing ratios, the magnitude of O_3 within the snow should consume most (if not all) of the NO produced. But the detection of NO in the upper layers of the snowpack suggest that O_3 is not the main sink for NO and other species must be acting as sink for O_3 within the firn.
- **NO_2 constitutes most of the NO_x at Summit and present a different distribution within the snowpack with respect to NO .** NO is mainly located within the first 20-50 cm of the snowpack most likely as a result of NO_2 photolysis. On the other hand, NO_2 is detected in large concentrations in levels deeper than 50 cm most likely as result of vertical transport, absence of light that could cause photolysis and absence of advection that could transport NO_2 out of the snow. These observations demonstrate that is necessary to include both physical and chemical processes in order to adequately describe

the distribution of NO_x within the snowpack and therefore the differences in snowpack chemistry at different layers.

- **NO_2 seasonal maximum is offset from radiation maximum levels, being detected during early spring while NO production correlates with radiation.** NO_2 maximum concentrations were detected in April, while NO production is directly related to radiation availability and thus its maximum is detected during months of high isolation (May-June-July). The offset of NO_2 is most likely to be an effect of the increase in NO production during late spring and summer seasons, suggesting that variations in radiation availability at photochemically active levels within the snow must be included in models that attempt to describe snowpack photochemistry, as NO_x variations will drive different chemical processes within the firn and/or the quasi-liquid layer.
- **NO_2 production occurs within the first centimeters of the snowpack and is further transported to layers underneath.** The analysis of diurnal cycles at the upper layers of the snowpack shows that NO_2 is produced at least in the first 20 cm of the snowpack, where maximum values correlate with the peak in radiation. In layers underneath, the maximum is observed at overnight suggesting that NO_2 detected at this depths is being transported from upper levels. At the end of the summer, the maximum is observed at late afternoon instead of midnight suggesting that a different mechanism takes place at the end of the season.
- **NO enhancements are detected deeper as radiation increases over the season.** First enhancements at 20 cm depth are detected during March while at 50 cm depth are measured in April. At both depths, NO enhancements reach maximum daily values at times of maximum insolation, which suggest that rather than transport being the main mechanism driving NO distribution, light can penetrate deeper within the snow and initiate photolytic processes at depths where at the beginning of the sunlight season no enhancements are detected.

5.2 Future work

The results presented in this work have provided a reliable estimation of the budget of NO_x within the snowpack at Summit as well as insight on the complex relationship between transport processes within the firn, physical characteristics of the snowpack, radiation availability at different depths and the distribution of trace gases within the snow. All these variables affect the distribution of nitrogen oxides within the firn, which in turn will affect the chemical processes governing snow chemistry. These long-term measurements will be a valuable input for models that attempt to describe the snow chemistry occurring in the firn and the quasi-liquid layer.

The next step will be the analysis of measurements of NO_x gradients above the snow and the determination of fluxes to the overlying atmosphere. The determination of relationships between patterns observed in the firn and variability in the emissions of these gases to the atmosphere will allow to fully characterize air-snow NO_x interactions at Summit.

Secondly, long-term measurements of other trace gases within the firn will help to interpret the observations that were presented here. NO_x and ozone are undoubtedly a key piece in the snow photochemistry of Summit, but previous studies have already detected during short campaigns that many other species such as Hg, H_2O_2 , CH_2O , halogens and hydrocarbons are present in the atmosphere above the snowpack at Summit. This study has already demonstrated that the firn sampling at a low flow rate can provide a reliable picture of the natural distribution of gases within the firn. Long-term measurements would contribute to understand the variability of the chemical processes governing air-snow interactions and therefore improve the representation of the mechanisms currently described in snow chemistry models.

Finally, the characterization of these processes at a global scale will need the study of air-snow interactions in different environments. Summit already constitutes a start point for the parameterization of snowpacks over glacial ice at polar regions. The continuation of these studies at sites with seasonal snow (such as alpine regions) or sites with snow over permafrost will allow to include interactions due to natural emissions from biological active surfaces beneath the snowpack, and subsequently to the atmosphere.

REFERENCES

- (1) Honrath R, Peterson M, Guo S, Dibb J, Shepson P, Campbell B, Evidence of NO_x production within or upon ice particles in the Greenland snowpack. *Geophysical Research Letters*. 1999;26(6):695–698.
- (2) Laj P, Palais J, Gardner J, Sigurdsson H, Modified HNO₃ seasonality in volcanic layers of a polar ice core: Snow-pack effect or photochemical perturbation? *Journal of Atmospheric Chemistry*. 1993;16(3):219–230.
- (3) Röthlisberger R, Hutterli M, Sommer S, Wolff E, Mulvaney R, Factors controlling nitrate in ice cores: Evidence from the Dome C deep ice core. *Journal of Geophysical Research*. 2000;105(D16):20565–20572.
- (4) Röthlisberger R, Hutterli M, Wolff E, Mulvaney R, Fischer H, Bigler M, Goto-Azuma K, Hansson M, Ruth U, Siggaard-Andersen M, *et al.*, Nitrate in Greenland and Antarctic ice cores: a detailed description of post-depositional processes. *Annals of Glaciology*. 2002;35(1):209–216.
- (5) Beine H, Domine F, Simpson W, Honrath R, Sparapani R, Zhou X, King M, Snow-pile and chamber experiments during the Polar Sunrise Experiment 'Alert 2000': exploration of nitrogen chemistry. *Atmospheric Environment*. 2002;36(15-16):2707–2719.
- (6) Dibb J, Talbot R, Munger J, Jacob D, Fan S, Air-snow exchange of HNO₃ and NO_y at Summit, Greenland. *Journal of Geophysical Research*. 1998;103(D3):3475–3486.
- (7) Helmig D, Oltmans S, Morse T, Dibb J, What is causing high ozone at Summit, Greenland?. *Atmospheric Environment*. 2007;41(24):5031–5043.

- (8) Honrath R, Lu Y, Peterson M, Dibb J, Arsenault M, Cullen N, Steffen K, Vertical fluxes of NO_x, HONO, and HNO₃ above the snowpack at Summit, Greenland. *Atmospheric Environment*. 2002;36(15-16):2629–2640.
- (9) Jacobi H, Bales R, Honrath R, Peterson M, Dibb J, Swanson A, Albert M, Reactive trace gases measured in the interstitial air of surface snow at Summit, Greenland. *Atmospheric Environment*. 2004;38(12):1687–1697.
- (10) Sumner A, Shepson P, Grannas A, Bottenheim J, Anlauf K, Worthy D, Schroeder W, Steffen A, Domine F, Perrier S, *et al.*, Atmospheric chemistry of formaldehyde in the Arctic troposphere at Polar Sunrise, and the influence of the snowpack. *Atmospheric Environment*. 2002;36(15-16):2553–2562.
- (11) Swanson A, Blake N, Dibb J, Albert M, Blake D, Sherwood Rowland F, Photochemically induced production of CH₃Br, CH₃I, C₂H₅I, ethene, and propene within surface snow at Summit, Greenland. *Atmospheric Environment*. 2002;36(15-16):2671–2682.
- (12) Beine H, Amoroso A, Domine F, King M, Nardino M, Ianniello A, France J, Surprisingly small HONO emissions from snow surfaces at Browning Pass, Antarctica. *Atmospheric Chemistry and Physics*. 2006;6(9):2569–2580.
- (13) Cotter E, Jones A, Wolff E, Bauguitte S, What controls photochemical NO and NO₂ production from Antarctic snow. Laboratory investigation assessing the wavelength and temperature dependence. *Journal of Geophysical Research*. 2003;108(D4):4147–4157.
- (14) Davis D, Nowak J, Chen G, Buhr M, Arimoto R, Hogan A, Eisele F, Mauldin L, Tanner D, Shetter R, *et al.*, Unexpected high levels of NO observed at South Pole. *Geophysical Research Letters*. 2001;28(19):3625–3628.
- (15) Davis D, Chen G, Buhr M, Crawford J, Lenschow D, Lefer B, Shetter R, Eisele F, Mauldin L, Hogan A, South Pole NO_x chemistry: an assessment of factors controlling variability and absolute levels. *Atmospheric Environment*. 2004;38(32):5375–5388.

- (16) Helmig D, Johnson B, Warshawsky M, Morse T, Neff W, Eisele F, Davis D, Nitric oxide in the boundary-layer at South Pole during the Antarctic Tropospheric Chemistry Investigation (ANTCI). *Atmospheric Environment*. 2008;42(12):2817–2830.
- (17) Hutterli M, McConnell J, Chen g, Bales R, Davis D, Lenschow D, Formaldehyde and hydrogen peroxide in air, snow and interstitial air at South Pole. *Atmospheric Environment*. 2004;38(32):5439–5450.
- (18) Bocquet F, Helmig D, Oltmans S, Ozone in interstitial air of the mid-latitude, seasonal snowpack at Niwot Ridge, Colorado. *Arctic, Antarctic, and Alpine Research*. 2007;39(3):375–387.
- (19) Helmig D, Seok B, Williams M, Hueber J, Sanford R, Fluxes and chemistry of nitrogen oxides in the Niwot Ridge, Colorado, snowpack. *Biogeochemistry*. 2009;95(1):115–130.
- (20) Honrath R, Peterson M, Dziobak M, Dibb J, Arsenault M, Green S, Release of NO_x from Sunlight-irradiated Midlatitude Snow. *Geophysical Research Letters*. 2000;27(15):2237–2240.
- (21) Boxe C and Saiz-Lopez A, Multiphase modeling of nitrate photochemistry in the quasi-liquid layer (QLL): implications for NO_x release from the Arctic and coastal Antarctic snowpack. *Atmospheric Chemistry and Physics*. 2008;8(2):4855–4864.
- (22) Cho H, Shepson P, Barrie L, Cowin J, Zaveri R, NMR investigation of the quasi-brine layer in ice/brine mixtures. *Journal of Physical Chemistry B*. 2002;106(43):11226–11232.
- (23) Kahan T, Kwamena N, Donaldson D, Different photolysis kinetics at the surface of frozen freshwater vs. frozen salt solutions. *Atmospheric Chemistry and Physics*. 2010;10:10917–10922.
- (24) Kahan T, Zhao R, Jumaa K, Donaldson D, Anthracene Photolysis in Aqueous Solution and Ice: Photon Flux Dependence and Comparison of Kinetics

- in Bulk Ice and at the Air- Ice Interface. *Environmental Science&Technology*. 2010;44(4):1302–1306.
- (25) Domine F and Shepson P, Air-snow interactions and atmospheric chemistry. *Science*. 2002;297(5586):1506.
 - (26) Grannas A, Jones A, Dibb J, Ammann M, Anastasio C, Beine H, Bergin M, Bottenheim J, Boxe C, Carver G, *et al.*, An overview of snow photochemistry: evidence, mechanisms and impacts. *Atmospheric Chemistry and Physics*. 2007;7(16):4329–4373.
 - (27) E. ACIA., Arctic Climate Impact Assessment. Cambridge University Press Cambridge, 2005.
 - (28) Seok B, Helmig D, Williams M, Liptzin D, Chowanski K, Hueber J, An automated system for continuous measurements of trace gas fluxes through snow: an evaluation of the gas diffusion method at a subalpine forest site, Niwot Ridge, Colorado. *Biogeochemistry*. 2009;95(1):95–113.
 - (29) Domine F, Albert M, Huthwelker T, Jacobi H, Kokhanovsky A, Lehning M, Picard G, Simpson W, Snow physics as relevant to snow photochemistry. *Atmospheric Chemistry and Physics*. 2008;8(2):171–208.
 - (30) Albert M and Shultz E, Snow and firn properties and air-snow transport processes at Summit, Greenland. *Atmospheric Environment*. 2002;36(15-16):2789–2797.
 - (31) Courville Z, Albert M, Fahnestock M, Cathles IV L, Shuman C, Impacts of an accumulation hiatus on the physical properties of firn at a low-accumulation polar site. *Journal of Geophysical Research*. 2007;112(F2):F02030.
 - (32) Simpson W, King M, Beine H, Honrath R, Peterson M, Atmospheric photolysis rate coefficients during the Polar Sunrise Experiment ALERT2000. *Atmospheric Environment*. 2002;36(15-16):2471–2480.

- (33) Simpson W, King M, Beine H, Honrath R, Zhou X, Radiation-transfer modeling of snow-pack photochemical processes during ALERT 2000. *Atmospheric Environment*. 2002;36(15-16):2663–2670.
- (34) King M and Simpson W, Extinction of UV radiation in Arctic snow at Alert, Canada (82 N). *Journal of Geophysical Research*. 2001;106(D12):12499.
- (35) Faraday M, On regelation, and on the conservation of force. *Philosophical Magazine*. 1859;17:162-169.
- (36) Dash J, Rempel A, Wettlaufer J, The physics of premelted ice and its geophysical consequences. *Reviews of Modern Physics*. 2006;78(3):695–741.
- (37) Boxe C and Saiz-Lopez A, Influence of thin liquid films on polar ice chemistry: Implications for Earth and planetary science. *Polar Science*. 2009;3(1):73–81.
- (38) Boxe C, Colussi A, Hoffmann M, Tan D, Mastromarino J, Case A, Sandholm S, Davis D, Multiscale ice fluidity in NO_x photodesorption from frozen nitrate solutions. *Journal of Physical Chemistry A*. 2003;107(51):11409–11413.
- (39) Dubowski Y, Colussi A, Hoffmann M, Nitrogen dioxide release in the 302 nm band photolysis of spray-frozen aqueous nitrate solutions. *Atmospheric implications*. *Journal of Physical Chemistry A*. 2001;105(20):4928–4932.
- (40) Dubowski Y, Colussi A, Boxe C, Hoffmann M, Monotonic increase of nitrite yields in the photolysis of nitrate in ice and water between 238 and 294 K. *Journal of Physical Chemistry A*. 2002;106(30):6967–6971.
- (41) Doppenschmidt A and Butt H, Measuring the thickness of the liquid-like layer on ice surfaces with atomic force microscopy. *Langmuir*. 2000;16(16):6709–6714.
- (42) Kahan T, Reid J, Donaldson d, Spectroscopic probes of the quasi-liquid layer on ice. *Journal of Physical Chemistry A*. 2007;111(43):11006–11012.
- (43) Jacobi H and Hilker B, A mechanism for the photochemical transformation of nitrate in snow. *Journal of Photochemistry and Photobiology A: Chemistry*. 2007;185(2-3):371–382.

- (44) Thomas J, Stutz J, Lefer B, Huey G, Toyota K, Dibb J, von Glasow R, Modeling chemistry in and above snow at Summit, Greenland–Part 1: Model description and results. *Atmospheric Chemistry and Physics Discussions*. 2010.
- (45) Voss L, Henson B, Wilson K, Robinson J, Atmospheric impact of quasiliquid layers on ice surfaces. *Geophysical Research Letters*. 2005;32:L0787–L0790.
- (46) Grannas A, Bausch A, Mahanna K, Enhanced aqueous photochemical reaction rates after freezing. *Journal of Physical Chemistry A*. 2007;111(43):11043–11049.
- (47) Ram K and Anastasio C, Photochemistry of phenanthrene, pyrene, and fluoranthene in ice and snow. *Atmospheric Environment*. 2009;43(14):2252–2259.
- (48) Legrand M and Mayewski P, Glaciochemistry of polar ice cores: a review. *Reviews of Geophysics*. 1997;35(3):219–243.
- (49) Honrath R, Guo S, Peterson M, Dziobak M, Dibb J, Arsenault M, Photochemical production of gas phase NO_x from ice crystal NO₃[−]. *Journal of Geophysical Research*. 2000;105(D19):24183–24190.
- (50) Mack J and Bolton J, Photochemistry of nitrite and nitrate in aqueous solution: a review. *Journal of Photochemistry and Photobiology A: Chemistry*. 1999;128(1-3):1–13.
- (51) Chu L and Anastasio C, Quantum yields of hydroxyl radical and nitrogen dioxide from the photolysis of nitrate on ice. *Journal of Physical Chemistry A*. 2003;107(45):9594–9602.
- (52) Chu L and Anastasio C, Temperature and wavelength dependence of nitrite photolysis in frozen and aqueous solutions. *Environmental Science&Technology*. 2007;41(10):3626–3632.
- (53) Zehavi D and Rabani J, Pulse radiolytic investigation of O[−]_{aq} radical ions. *Journal of Physical Chemistry*. 1971;75:1738–1744.
- (54) Sander R, Compilation of Henry’s law constants for inorganic and organic species of potential importance in environmental chemistry. Max-Planck Institute of Chemistry, Air Chemistry Dept., 1999.

- (55) Boxe C, Colussi A, Hoffmann M, Murphy J, Wooldridge P, Bertram T, Cohen R, Photochemical production and release of gaseous NO₂ from nitrate-doped water ice. *Journal of Physical Chemistry A*. 2005;109(38):8520–8525.
- (56) Bock J and Jacobi H, Development of a Mechanism for Nitrate Photochemistry in Snow. *Journal of Physical Chemistry A*. 2010;114(4):1790–1796.
- (57) Park J and Lee Y, Solubility and decomposition kinetics of nitrous acid in aqueous solution. *The Journal of Physical Chemistry*. 1988;92(22):6294–6302.
- (58) Anastasio C and Chu L, Photochemistry of Nitrous Acid (HONO) and Nitrous Acidium Ion (H₂ONO⁺) in Aqueous Solution and Ice. *Environmental Science&Technology*. 2009;43(4):1108–1114.
- (59) Beine H, Colussi A, Amoroso A, Esposito G, Montagnoli M, Hoffmann M, HONO emissions from snow surfaces. *Environmental Research Letters*. 2008;3:045005–045011.
- (60) Pinzer B, Kerbrat M, Huthwelker T, Gaggeler H, Schneebeli M, Ammann M, Diffusion of NO_x and HONO in snow: A laboratory study. *Journal of Geophysical Research*. 2010;115(D3):D03304.
- (61) George C, Strekowski R, Kleffmann J, Stemmler K, Ammann M, Photoenhanced uptake of gaseous NO₂ on solid organic compounds: a photochemical source of HONO? *Faraday Discussions*. 2005;130:195–210.
- (62) Hellebust S, O’Sullivan D, Sodeau J, Protonated Nitrosamide and Its Potential Role in the Release of HONO from Snow and Ice in the Dark. *Journal of Physical Chemistry A*. 2010;111:1167–1171.
- (63) Simpson W, Von Glasow R, Riedel K, Anderson P, Ariya P, Bottenheim J, Burrows J, Carpenter L, Frieb U, Goodsite M, *et al.*, Halogens and their role in polar boundary-layer ozone depletion. *Atmospheric Chemistry and Physics*. 2007;7(2):4375–4418.

- (64) Dibb J, Ziemba L, Luxford J, Beckman P, Bromide and other ions in the snow, firn air, and atmospheric boundary layer at Summit during GSHOX. *Atmospheric Chemistry and Physics*. 2010;10:19931–19942.
- (65) Peterson M and Honrath R, Observations of rapid photochemical destruction of ozone in snowpack interstitial air. *Geophysical Research Letters*. 2001;28(3):511–514.
- (66) Fain X, Ferrari C, Dommergue A, Albert M, Battle M, Arnaud L, Barnola J, Cairns W, Barbante C, Boutron C, Mercury in the snow and firn at Summit Station, Central Greenland, and implications for the study of past atmospheric mercury levels. *Atmospheric Chemistry and Physics*. 2008;8:3441–3457.
- (67) Helmig D, Johnson B, Oltmans S, Neff W, Eisele F, Davis D, Elevated ozone in the boundary layer at South Pole. *Atmospheric Environment*. 2008;42(12):2788–2803.
- (68) Albert M, Grannas A, Bottenheim J, Shepson P, Perron F, Processes and properties of snow-air transfer in the high Arctic with application to interstitial ozone at Alert, Canada. *Atmospheric Environment*. 2002;36(15-16):2779–2787.
- (69) Helmig D, Bocquet F, Cohen L, Oltmans S, Ozone uptake to the polar snowpack at Summit, Greenland. *Atmospheric Environment*. 2007;41(24):5061–5076.
- (70) Chu L and Anastasio C, Formation of hydroxyl radical from the photolysis of frozen hydrogen peroxide. *Journal of Physical Chemistry A*. 2005;109(28):6264–6271.
- (71) Anastasio C, Galbavy E, Hutterli M, Burkhart J, Friel D, Photoformation of hydroxyl radical on snow grains at Summit, Greenland. *Atmospheric Environment*. 2007;41(24):5110–5121.
- (72) Sumner A and Shepson P, Snowpack production of formaldehyde and its effect on the Arctic troposphere. *Nature*. 1999;398(6724):230–233.
- (73) Grannas A, Shepson P, Filley T, Photochemistry and nature of organic matter in Arctic and Antarctic snow. *Global Biogeochemical Cycles*. 2004;18(1):GB1006.

- (74) Blunier T, Floch G, Jacobi H, Quansah E, Isotopic view on nitrate loss in Antarctic surface snow. *Geophysical Research Letters*. 2005;32:13501.
- (75) Frey M, Savarino J, Morin S, Erbland J, Martins J, Photolytic control of the nitrate stable isotope signal in snow and atmosphere of East Antarctica and implications for reactive nitrogen cycling. *Atmospheric Chemistry and Physics*. 2009;9:8681–8696.
- (76) Hastings M, Steig E, Sigman D, Seasonal variations in N and O isotopes of nitrate in snow at Summit, Greenland: Implications for the study of nitrate in snow and ice cores. *Journal of Geophysical Research*. 2004;109(D20):D20306.
- (77) Jarvis J, Steig E, Hastings M, Kunasek M, Influence of local photochemistry on isotopes of nitrate in Greenland snow. *Geophysical Research Letters*. 2008;35(21):L21804.
- (78) Bowling D, Massman W, Schaeffer S, Burns S, Monson R, Williams M, Biological and physical influences on the carbon isotope content of CO₂ in a subalpine forest snowpack, Niwot Ridge, Colorado. *Biogeochemistry*. 2009;95(1):37–59.
- (79) Peterson M, Honrath R, Parrish D, Oltmans S, Measurements of nitrogen oxides and a simple model of NO_y fate in the remote North Atlantic marine atmosphere. *Journal of Geophysical Research*. 1998;103(D11):13489–13503.
- (80) Peterson M and Honrath R, NO_x and NO_y over the northwestern North Atlantic: Measurements and measurement accuracy. *Journal of Geophysical Research*. 1999;104:11–695.
- (81) Kley D and McFarland M, Chemiluminescence detector for NO and NO₂. *Atmospheric Technology*. 1980;12.
- (82) Atkinson R, Baulch D, Cox R, Crowley J, Hampson R, Hynes R, Jenkin M, Rossi M, Troe J, Evaluated kinetic and photochemical data for atmospheric chemistry: Volume I-Gas phase reactions of Ox, HOx, NO_x and SO_x species. *Atmospheric Chemistry and Physics*. 2004;4:1461–1738.

- (83) Qiu R, Green S, Honrath R, Peterson M, Lu Y, Dziobak M, Measurements of $J_{\text{NO}_3^-}$ in snow by nitrate-based actinometry. *Atmospheric Environment*. 2002;36(15-16):2563–2571.
- (84) Peterson M, Barber D, Green S, Monte Carlo modeling and measurements of actinic flux levels in Summit, Greenland snowpack. *Atmospheric Environment*. 2002;36(15-16):2545–2551.
- (85) Albert M and Hawley R, Seasonal changes in snow surface roughness characteristics at Summit, Greenland: Implications for snow and firn ventilation. *Annals of Glaciology*. 2002;35(1):510–514.
- (86) Albert M, Modeling heat, mass, and species transport in polar firn. *Annals Of Glaciology*. 1996.
- (87) Bartels-Rausch T, Eichler B, Zimmermann P, Gaggeler H, Ammann M, The adsorption enthalpy of nitrogen oxides on crystalline ice. *Atmospheric Chemistry and Physics*. 2002;2:235–247.
- (88) Bartels-Rausch T, Brigante M, Elshorbany Y, Ammann M, D’Anna B, George C, Stemmler K, Ndour M, Kleffmann J, Humic acid in ice: Photo-enhanced conversion of nitrogen dioxide into nitrous acid. *Atmospheric Environment*. 2010;44:5443–5450.
- (89) Cohen L, Helmig D, Neff W, Grachev A, Fairall C, Boundary-layer dynamics and its influence on atmospheric chemistry at Summit, Greenland. *Atmospheric Environment*. 2007;41(24):5044–5060.
- (90) Solomon S, Portmann R, Thompson D, Contrasts between antarctic and arctic ozone depletion. *Proceedings of the National Academy of Sciences*. 2007;104(2):445.
- (91) N. O. Earth System Research Laboratory, Global Monitoring Division and A. Administration, Ozone vertical profiles Summit, Greenland. Available from <http://www.esrl.noaa.gov/gmd/dv/iadv/>

- (92) Burkhart J, Hutterli M, Bales R, McConnell J, Seasonal accumulation timing and preservation of nitrate in firn at Summit, Greenland. *Journal of Geophysical Research*. 2004;109:D19302.
- (93) Kim S and Kang H, Efficient Conversion of Nitrogen Dioxide into Nitrous Acid on Ice Surfaces. *Journal of Physical Chemistry Letters*. 2010;1:3085–3089.
- (94) Gao R, Keim E, Woodbridge E, Ciciora S, Proffitt M, Thompson T, McLaughlin R, Fahey D, New photolysis system for NO_2 measurements in the lower stratosphere. *Journal of Geophysical Research*. 1994;99(D10):20673.
- (95) Peterson M, Nitrogen oxides in the remote North Atlantic troposphere: Measurements and diagnostic modeling. PhD thesis, 1999.

APPENDICES

APPENDIX A. SCHEMATICS

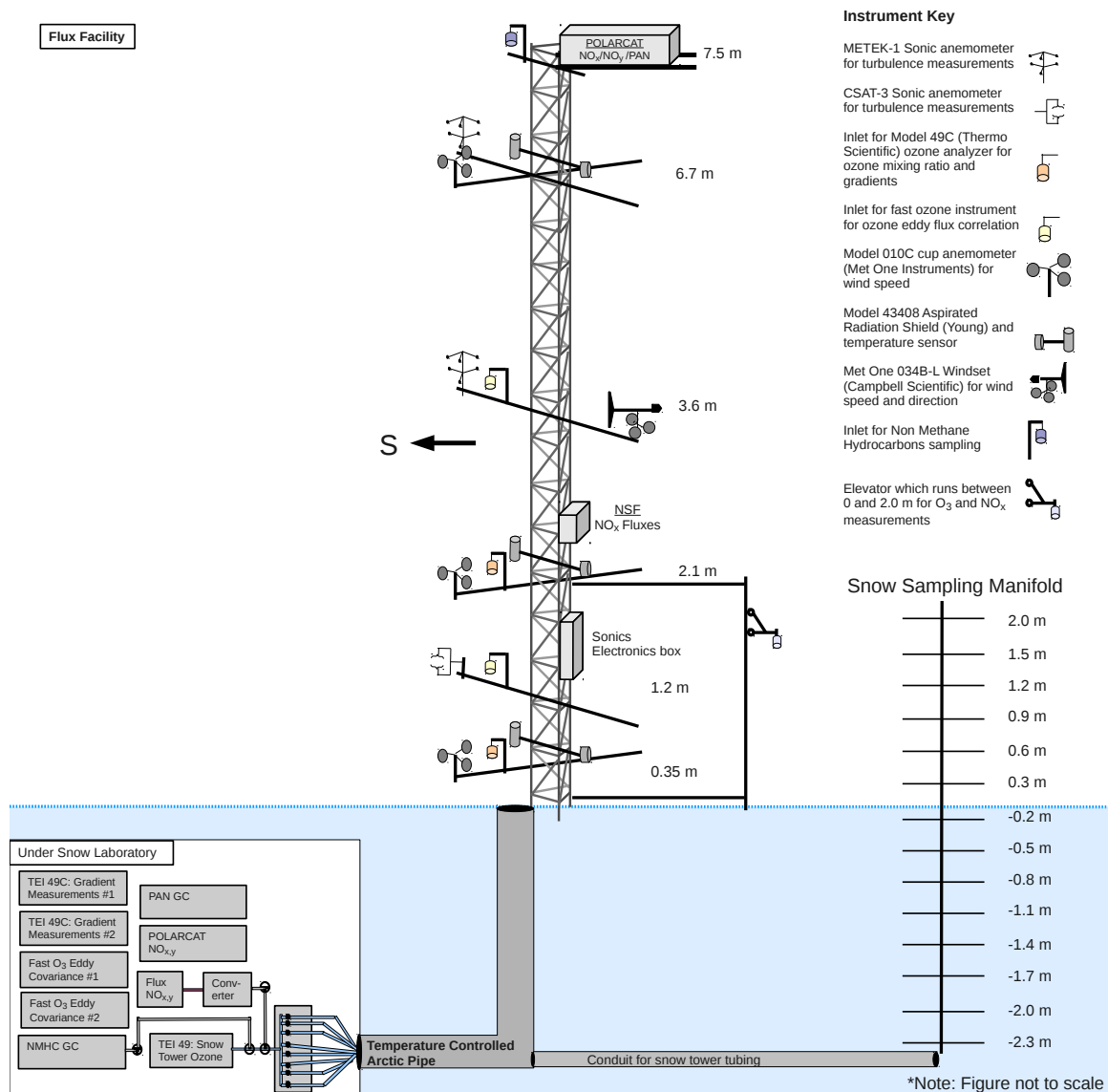


Figure A.1. Detailed Schematic of the Experimental Setup including the snowtower extension. Note that this figure is not to scale. (Adapted from the work of Brie Van Dam, INSTAAR)



APPENDIX B. DERIVATION OF RELEVANT EQUATIONS USED FOR THIS WORK.

B.1 Derivation of the Equation for Calculating the NO₂ Sensitivity

The NO₂ sensitivity of the instrument, which was used to calculate NO₂ mixing ratio, was calculated from parameters measured during calibrations. The derivation begins with the equation of NO₂ mixing ratio and NO₂ sensitivity given by Gao et al. (94) and Peterson (95).

$$[\text{NO}_2]_a = \frac{\overbrace{(\text{NO}_2 \text{ channel signal} - \text{NO}_2 \text{ channel background})}^{\text{signal due to NO}_2 \text{ and NO}} - \overbrace{([\text{NO}]_a \cdot S_{\text{NO}}|^{\text{ON}})}^{\text{signal due to NO}}}{S_{\text{NO}_2}} \quad (\text{B.1})$$

where:

$[\text{NO}_2]_a$ = ambient NO₂ mixing ratio (pptv)

$[\text{NO}]_a$ = ambient NO mixing ratio (pptv)

$S_{\text{NO}}|^{\text{ON}}$ = sensitivity of NO while the NO₂ converter is ON (cps pptv⁻¹)

Equation B.1 is solved for the NO₂ sensitivity. and can be rewritten using parameters measured during the automated calibrations:

$$S_{\text{NO}_2} = \frac{\overbrace{(\text{NO}_X/\text{C}/\text{UV} - \text{NO}/\text{Z})}^{\text{signal due to NO}_2 \text{ and NO}} - \overbrace{([\text{NO}]_{\text{cal}}^{\text{UV}} - [\text{NO}]_a) \cdot S_{\text{NO}}|^{\text{ON}}}_{\text{signal due to NO}}}{[\text{NO}]_{\text{cal}}^{\text{UV}} + [\text{NO}]_a} \quad (\text{B.2})$$

where:

$$\begin{aligned}
\text{NO}_X/\text{C}/\text{UV} &= \text{PMT signal with NO}_2 \text{ converter ON from standard addition of} \\
&\quad [\text{NO}]_{\text{cal}}^{\text{UV}} \text{ and } [\text{NO}_2]_{\text{cal}}^{\text{UV}} \text{ (cps)} \\
\text{NO}/\text{Z} &= \text{background PMT signal with NO}_2 \text{ converter OFF (assumed equal to} \\
&\quad \text{background PMT signal with NO}_2 \text{ converter ON) (cps)} \\
[\text{NO}]_{\text{cal}}^{\text{UV}} &= \text{mixing ratio of NO calibration gas remaining while the NO}_2 \\
&\quad \text{converter is ON (pptv)} \\
[\text{NO}_2]_{\text{cal}}^{\text{UV}} &= \text{mixing ratio of NO}_2 \text{ created by conversion of the NO calibration gas} \\
&\quad \text{while the NO}_2 \text{ converter is ON (pptv)}
\end{aligned}$$

Use of NO/Z instead of NO/Z_{true} will cause less than 0.1% of error if [NO]_a is less than 446 ppt. In addition,

$$[\text{NO}_2]_{\text{cal}}^{\text{UV}} = [\text{NO}]_{\text{cal}} - [\text{NO}]_{\text{cal}}^{\text{UV}} \quad (\text{B.3})$$

where:

[NO]_{cal} = standard addition mixing ratio of the unmodified NO calibration gas (pptv)

The sensitivity of NO with the NO₂ converter ON is given by:

$$S_{\text{NO}}|_{\text{ON}} = \frac{\text{NO}_X/\text{C} - \text{NO}_X/\text{M}}{[\text{NO}_{\text{cal}}]} \quad (\text{B.4})$$

where:

NO_X/C = PMT signal with NO₂ converter ON during
standard addition of [NO]_{cal} (cps)

NO_X/M = PMT signal with NO₂ converter ON due to ambient NO and NO₂ (cps)

and:

$$[\text{NO}_2]_{\text{cal}}^{\text{UV}} = \frac{\text{NO}/\text{C} - \text{NO}/\text{C}/\text{UV}}{S_{\text{NO}}|_{\text{OFF}}} \quad (\text{B.5})$$

where:

NO/C/UV = PMT signal with NO₂ converter OFF from standard addition
of [NO]_{cal}^{UV} (cps)
NO/C = PMT signal with NO₂ converter OFF during standard addition
of [NO]_{cal} (cps)

The sensitivity of NO with the NO₂ converter OFF is given by:

$$S_{NO}|^{OFF} = \frac{NO/C - NO/M}{[NO]_{cal}} \quad (B.6)$$

where:

NO/M = PMT signal with NO₂ converter OFF due to actual NO (cps)

Then, the sensitivity of NO₂ is given by:

$$S_{NO_2} = \frac{\left(\overbrace{(NO_X/C/UV - NO/Z)}^{\text{signal due to NO}_2 \text{ and NO}} - \overbrace{\left(\frac{NO/C/UV - NO/Z}{NO/C - NO/M} \right) \cdot (NO_X/C - NO_X/M)}^{\text{signal due to NO}} \right)}{[NO_2]_{cal}^{UV} + [NO_2]_a} \quad (B.7)$$

and:

$$[NO]_a = \frac{NO/M - NO/Z}{S_{NO}|^{OFF}} \quad (B.8)$$

$$[NO_2]_a = \frac{\left(\frac{NO_X/M - NO/Z}{FrcZrd} \right) - [NO]_a \cdot S_{NO}|^{ON}}{S_{NO_2}} \quad (B.9)$$

where:

FrcZrd = fraction of NO removed by the zeroing procedure

$$FrcZrd = 1 - \frac{NO/C/Z - NO/Z}{NO/C - NO/M} \quad (B.10)$$

Substituting Equations B.6 and B.8 into Equation B.9 yields:

$$[\text{NO}_2]_a = \frac{(\text{NO}_X/\text{M} - \text{NO}/\text{Z}) - \frac{(\text{NO}/\text{M} - \text{NO}/\text{Z})(\text{NO}_X/\text{C} - \text{NO}_X/\text{M})}{\text{NO}/\text{C} - \text{NO}/\text{M}}}{S_{\text{NO}_2} \cdot \text{FrcZrd}} \quad (\text{B.11})$$

Substituting Equations B.5, B.6 and B.11 into Equation B.7 yields:

$$S_{\text{NO}_2} = \frac{(\text{NO}_X/\text{C}/\text{UV} - \text{NO}_X/\text{M}) - \frac{(\text{NO}/\text{C}/\text{UV} - \text{NO}/\text{M})(\text{NO}_X/\text{C} - \text{NO}_X/\text{M})}{(\text{NO}/\text{C} - \text{NO}/\text{M})\text{FrcZrd}}}{\frac{(\text{NO}/\text{C} - \text{NO}/\text{C}/\text{UV})[\text{NO}]_{\text{cal}}}{\text{NO}/\text{C} - \text{NO}/\text{M}}} \quad (\text{B.12})$$

If the FrcZrd in Equation B.12 is ignored, the error will be less than 0.1% if $[\text{NO}_2]_a$ is less than 428 ppt. Therefore the equation used in the IDL procedure is given below:

$$S_{\text{NO}_2} = \frac{(\text{NO}/\text{C} - \text{NO}/\text{M})(\text{NO}_X/\text{C}/\text{UV} - \text{NO}_X/\text{M}) - (\text{NO}/\text{C}/\text{UV} - \text{NO}/\text{M})(\text{NO}_X/\text{C} - \text{NO}_X/\text{M})}{(\text{NO}/\text{C} - \text{NO}/\text{C}/\text{UV}) * [\text{NO}]_{\text{cal}}} \quad (\text{B.13})$$

B.2 Derivation of the Equation for Correcting NO Sensitivity.

Equation 3.5 used for the linear fit analysis between NO sensitivity (SNO) and ambient O_3 is derived from the integrated rate law for equation 3.4 (equation 3.6) , presented now in equation B.14.

$$[NO] = [NO]_o \times \exp^{-k t [O_3]} \quad (B.14)$$

where $[NO]$ is the detected mixing ratio, k is the rate constant for reaction 3.4, t is the residence time in the sampling line, $[O_3]$ is the O_3 mixing ratio at the time of the measurement and $[NO]_o$ is the NO mixing ratio at the inlet, before any loss due to O_3 .

Rearranging and applying natural logarithm at both sides of the equation produces

$$\ln \frac{[NO]}{[NO]_o} = -k [NO] [O_3] t \quad (B.15)$$

Linearizing equation B.15 gives

$$\ln [NO] = \ln [NO]_o - k [NO] [O_3] t \quad (B.16)$$

Conditions at Summit allow to assume safely that $[NO]$ is sufficiently small compared to $[O_3]$ to express the rate constant k as a pseudo-first order rate constant k' , equivalent to $k [NO]$. Then, equation B.16 is expressed as

$$\ln [NO] = \ln [NO]_o - k' [O_3] t \quad (B.17)$$

Finally, since $\frac{[NO]}{[NO]_o} \equiv \frac{SNO}{SNO_o}$ is possible to express equation B.16 in terms of NO sensitivity (SNO) as follows

$$\ln [SNO] = \ln [SNO]_o - k' [O_3] t \quad (B.18)$$